remote sensing

MDPI

Review

Surface Roughness in Geomorphometry: From Basic Metrics Toward a Coherent Framework

Sebastiano Trevisani [1,*] and Peter L. Guth [2]

[1] Dipartimento di Culture del Progetto, University IUAV of Venice, Dorsoduro 2206, 30123 Venice, Italy
[2] Department of Oceanography, US Naval Academy, Annapolis, MD 21402, USA; prof.pguth@gmail.com
* Correspondence: strevisani@iuav.it

Highlights

What are the main findings?

- Surface roughness in geomorphometry is generally interpreted in the wider sense of surface texture
- Deep interrelations between surface roughness analysis, computer vision and surface metrology

What are the implications of the main findings?

- Need for benchmark data, represented by collection of DEM tiles with characteristic terrain patterns
- Need for participatory approaches for developing a coherent theorical and methodological framework for surface texture analysis in geomorphometry

Abstract

Surface roughness (SR), most often computed from a digital elevation model (DEM), is a fundamental concept in geomorphometry, with significant applications across the earth sciences and ecology. However, its analysis remains fragmented, lacking a unified conceptual and methodological framework within geomorphometry. This review synthesizes the current state of surface roughness research, highlighting persistent challenges that stem from this disunity. Key issues include a pervasive lack of consensus on terminology and definitions, frequent misuse of standardized indices, and difficulty in selecting appropriate analytical scales and metrics for specific landscapes and research questions. A major impediment to progress is the absence of benchmark datasets, which are crucial for the rigorous evaluation and comparison of both established and novel roughness metrics. Furthermore, we argue that in geomorphometry, roughness is best conceptualized as surface texture (ST), encompassing a multitude of terrain patterns across scales. Consequently, effective analysis often requires multiscale approaches and the development of new indices capable of quantifying specific textural features. We emphasize, for instance, the need for metrics based on robust statistical estimators, such as MAD or the Radial Roughness Index (RRI), to reliably characterize complex, heterogeneous terrain derived from high-resolution DEMs. These arguments are substantiated with computational examples comparing a range of metrics, from popular basic indices to more complex alternatives. This review aims to consolidate discourse on surface roughness and chart a path toward more robust, standardized, and interpretative analytical practices.

Keywords: DEM; geomorphometry; landform; pattern; roughness; ruggedness; rugosity; terrain; texture; waviness

Academic Editor: Tomaž Podobnikar

Received: 3 October 2025
Revised: 24 November 2025
Accepted: 27 November 2025
Published: 28 November 2025

Citation: Trevisani, S.; Guth, P.L. Surface Roughness in Geomorphometry: From Basic Metrics Toward a Coherent Framework. *Remote Sens.* **2025**, *17*, 3864. https://doi.org/10.3390/rs17233864

1. Introduction

Surface roughness (SR), despite ambiguities in its definition, is a key concept in multiple fields of sciences and engineering, with increased interest in recent decades. This is true also in earth sciences [1,2] and related disciplines such as ecology [3,4]. SR analysis contributes to the characterization and modeling of surface processes [2,5–7] and the understanding of morphogenetic factors, including the interactions with ecological processes. The increasing number of studies concerning SR in earth sciences is fueled by two main motivations. Technological innovations in remote sensing (e.g., lidar, radar, photogrammetry, etc.) permit measuring and representing the surface topography with a high level of detail and accuracy. SR analysis is conducted mostly by means of geomorphometric approaches [8–11] applied to digital elevation models (DEMs). The other motivation is related to the increasing need to characterize terrestrial, marine, and extra-terrestrial surfaces for a variety of scientific and practical reasons.

The analysis of SR provides relevant information concerning the geoenvironmental processes being studied or modeled. In terrestrial and extraterrestrial geomorphometry, SR characterization is relevant for multiple aspects, such as to infer material properties, study current or past processes, and evaluate the time elapsed since formation (e.g., [1,12–17]). SR can provide interesting information on geomorphic factors for geomorphological, geostructural, and ecological studies [1,3,18–21]. The quantification of SR can be particularly relevant for deriving impedance factors to multiple physical and biological processes, such as water/sediment flow, river and sea flood modeling, landslides, and movement of animal species [2,4,13,22–27]. SR-related indices can provide interpretable and relevant input features for machine learning (ML), for both unsupervised (e.g., k-means clustering for morphometric analysis, [28–30]) and supervised predictive learning approaches (e.g., random forest [31,32]). SR has been used as predictor variable in disciplines related to natural hazards, such as for the semi-automatic mapping of landforms [33–35], snow avalanches susceptibility [36], landslide susceptibility mapping [37], and wildfire susceptibility modeling [38]. In the marine environment, SR directly relates to biodiversity, and various measures of SR have also become a widely used proxy for benthic habitat and seabed geodiversity [39–42]. Even in the built environment roughness matters, for example, urban climatology studies focusing on wind and turbulence observations have used SR indices for identifying the wind profile within an urban environment [43]. Multiscale analysis of SR, conducted on digital terrain models (DTMs) and on digital surface models (DSMs) is relevant in the analysis of the energy production potential of wind turbines [44,45], in glaciological studies [46], and even in the analysis of damages induced on forests by storms and other extreme weather events [47].

Despite the relevance of SR analysis in earth sciences and the multitude of related applications, it is generally not considered as a specific and self-contained branch of geomorphometry. SR-related research has evolved in a fragmented and non-synergic way, according to a variety of approaches, algorithms, and interpretations. Most of the time, the characterization of SR is represented by calculating some local surface parameters, LSPs [8,11], somewhat related to the local surface variability. This has led to a suboptimal evolution of the field, with many aspects that can be improved and clarified, possibly according to a unifying theoretical framework.

1.1. Definitional Ambiguities

The first aspect that needs clarification is the definition of the term "surface roughness" [48] from a geomorphometric perspective. In fact, "roughness", similarly to "ruggedness", is a buzzword often computed and used without a clear definition. Hobson (1972) stated [48] (reprinted in [49]): "*A single concise definition of surface roughness is probably im-*

possible. The only usable definitions are incomplete because they describe only a few of the physical or mathematical properties of a surface. There may be as many of these definitions as there are roughness studies themselves." Most of the time SR is presented as a measure of complexity or heterogeneity of surface morphology [3,8,11,22,50]. The related indices are often defined according to an heuristic approach and seldom following a theoretical framework [8,48]. Sometimes SR is strictly connected with fractal theory, with which it shares a fascinating perspective on earth surface spatial pattern analysis [1,51–54]. Geostatistics [55–57], which focuses on the spatial–statistical variability structure of spatial fields, is naturally concerned with SR. The concept of spatial continuity of a 2D surface is directly related to its level of smoothing/regularization, and thus to its roughness. Even considering simple bivariate spatial continuity indices such as the variogram [55], it is evident that SR is something complex, characterized, for example, by multiscalarity and directionality [30,58,59]. The discourse can be moved further considering multipoint spatial–statistical indices [60], which describe more complex spatial patterns. A similar interpretation can be formulated considering spectral approaches based on Fourier analysis [12,61,62] and wavelets analysis [63–65].

The definition ambiguities are unavoidable to some extent, but some form of consensus on terminology should be found. Multiple SR-related terms are adopted, such as "fabric" [66] "grain" [8,48,67], "ruggedness" [3,4] "rugosity" [50], "texture" [8,28], and others (e.g., [1,15,39]). The interpretation of these terms is generally related to the scale, the terrain features to be highlighted, and different authors may have different interpretations for the same term. The interpretation of these terms is also related to disciplinary traditions. For instance, in geomorphology, "roughness" generally refers to fine-scale texture, while "ruggedness" is referred to longer-range undulations. From a geomorphometric perspective, and considering algorithms, the interpretation of these two terms can be different (Section 4), and their distinction can be somewhat ephemeral. For this reason, if not otherwise stated, we will use throughout the text terminology referring to the geomorphometric and algorithmic interpretation. Some scholars [11,22,68] describe surface roughness as a metric related to surface (or "topographic", "terrain", etc.) "complexity", inheriting all the fuzziness related to the term "complexity", both in the common sense as well as from a mathematical perspective. One may ask if a horizontal surface with some fine-grain roughness is more complex than a smooth folded quadratic surface. The geomorphometric meaning of the term "topographic complexity" should be defined first, which is a future project. In addition, many conventional SR indices are relatively simple measures of the overall spatial–statistical variability structure of a surface and cannot provide real information on complexity. We think that complexity of topography should not be interpreted just in the sense of overall statistical dispersion of height values [1,69–71]. An expression of complexity can be, for example, the coalescence of heterogenous morphological features with multiple wavelengths or the presence of curvilinear spatial patterns. Another example can be represented by multifractal behavior, with the presence of self-similar or self-affine morphological patterns, at least for a given range of scales and within specific spatial domains [1,53,70]. A final example of complexity is the presence of periodic structures, such as ripples and dune fields, which are often asymmetrical [72–74]. The complexity of terrain patterns manifests at multiple scales, and hence multiscale approaches are deeply interlinked with SR analysis.

1.2. Surface Texture

The earth science literature, including Hobson [48], implicitly interprets SR in the wider sense of "surface texture" (ST), not to be confused with the specific definition reported in earlier geomorphometric works (e.g., [8]) or with the specific metric used [28].

A compact plain language definition of texture from the Oxford Advanced Learner's dictionary is "the way that something feels when you touch it". ST, even if there is still some fuzziness, is an intuitive concept related to human visual and tactile perception of a surface and links directly to approaches adopted in surface metrology [75,76] and computer vision [77]. Moreover, when the 3D surface is represented as a gridded 2D scalar field there is complete convergence between ST and image texture (IT). Intuitively, ST may imply the presence of some repetitive and characteristic pattern. Connecting the concepts of landform [78,79] and terrain patterns [69,80], what constitutes SR/ST changes according to the scale of observation versus the scale of morphological features. A given local ST can be represented by an ensemble of landforms such as a set of drumlins or can be an internal characteristic of a specific landform, like parallel gullies along the slopes of a moraine. The spatial repetition of a characteristic terrain pattern should not be considered mandatory. In fact, the real surfaces are often characterized by singular and not repetitive spatial patterns that are very distinctive elements of topographic signature [9,79]. An example of these morphological features are punctual discontinuities such as hoodoos, local outliers, or hotspots from a geostatistical perspective, and linear features like scarps or lineaments. From a computational perspective, the analysis of roughness for these features may essentially be reduced to outliers and edge detection [81]. Unfortunately, the definition of a threshold in spatial variability for defining a given morphological feature as a discontinuity is not trivial and it is application-dependent, including the scale of analysis.

Given these considerations, the term SR is intended here as a synonym of ST, hence referring to the overall spatial variability structure of surfaces or, expressed in another terms, to the terrain patterns, independently from the scale of observation. This terminological choice is related to the general interpretation and use of the term SR in earth sciences and ecology literature. According to this interpretation, SR is intended differently from the surface metrology discipline [75], where SR is considered a specific aspect of ST (i.e., what it is left after removing the form/structure of the object), referring to the short-range spatial variability (Figure 1). Another ST characteristic is the waviness (Figure 1) that is relative to repetitive longer-range undulations, not far from similar morphologies related to aeolian and fluvial processes, such as dunes and ripples, e.g., ref. [74]. In surface metrology, the analysis of ST and of its components, such as SR and waviness, is highly standardized, including national and international standards [82,83] regarding the different metrics. However, even in this highly codified field there is an unavoidable ambiguity in terminology related to the scale of analysis with respect to the scale of morphological features analyzed. Depending on the scale of observation, what is interpreted as waviness at one scale can be interpreted as roughness when observing a larger spatial domain. The decision to use SR as synonym of ST, as implicitly formulated by Hobson [48], implies that to fully characterize the different aspects SR, a wide range of metrics is necessary, not just one "roughness index" [1,8,48]. Moreover, it makes little sense to talk about the best roughness index; however, one may ask which roughness index is best for describing a specific aspect of ST.

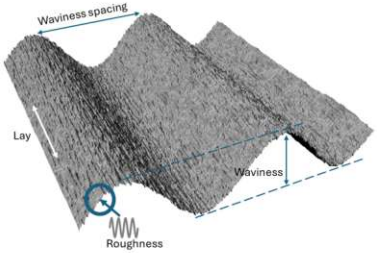

Figure 1. Surface texture and its main constituents according to surface metrology, supposing a planar form (i.e., structure): waviness, lay (anisotropy), and roughness. The interpretation is scale-dependent; the represented roughness (short-range irregularities) can be viewed as waviness at finer scale. Figure redrawn and redesigned from [84].

In Appendix E, we provide a glossary that defines and interprets key terms adopted in the paper.

1.3. A Plethora of Algorithms

Another element contributing to the current fragmentation in SR analysis in geomorphometry is related to the heterogeneity of mathematical and computational approaches that can be adopted [1,15,64]. The study of ST analyzes spatial data and hence it is not surprising that it touches many fields of science and technology, such as time series analysis, spatial statistics, pattern recognition, and image analysis. It is impossible to list and compare all the published approaches, due to the extremely wide literature and the lack of standard benchmark datasets for comparing and describing SR indices (see Section 3.2). In addition, there is not currently a synergic theoretical framework to link and compare the different perspectives and approaches in ST analysis in geomorphometry. Such a framework should provide a unifying view, fulfilling a basic requirement in geomorphometry for the interpretability of computed geomorphometrics. In fact, ST indices should be interpretable from a geomorphological and geoenvironmental viewpoint, or should at least describe specific and visually recognizable aspects of terrain texture. SR indices could be capable of detecting preferential orientations, curvilinear features, asymmetries, periodic structures, and related parameters like wavelength and amplitude and size and density of assemblages of features with varying sizes/amplitudes.

In this discussion we focus on widely adopted approaches available in GIS software like ArcGIS Pro (v3.6), Grass (v8), Microdem (Nov. 2025), SAGA (v9), and WhiteboxTools (2.4) and programming languages like Python (3.12)or R (4.5.2) and mainly based on relatively compact algorithms in terms of parameters and user's selections required to perform the analysis. We have made this decision to keep the analysis focused and tractable within the confines of a single article, and because end-users generally prefer simpler algorithms that require little tuning of parameters and are easily interpretable. More complex approaches, such as those based on geostatistics and spectral analysis, are flexible and have wide potential. However, they require many user decisions, often based on subjective criteria and application-dependent requirements, making the comparison between different approaches difficult. Despite the simplicity of most popular SR indices, they are often applied blindly, without recognizing the underlying limitations and char-

acteristics of the information provided. It is necessary to clarify their characteristics and behavior in specific morphological settings. More complex approaches are often based on the iterations at multiple scales of these basic indices.

1.4. Purposes of This Review

This review focuses on the geomorphometric computation of SR from DEMs; it is not intended to provide a general discussion on SR's significance in earth sciences [1,2], such as its role in the analysis and modeling of geomorphological and geological processes. In summary, the general aim of this review is to discuss some of the criticalities and main aspects that should be improved to boost progress in this exciting field of inquiry. The specific objectives are represented by the following points:

- Highlight the key challenges and complexities underlying SR analysis, including the limitations of the raster representation of morphology. This includes emphasizing the issues concerning the scale of analysis and the need for multiscale approaches.
- Provide an overview of a wide set of popular SR indices, highlighting the information provided and their intrinsic limitations.
- Present examples on how these limitations can be easily isolated and overcome by adopting a more structured methodological framework.
- Discuss the need for an atlas with DEMs showing examples of characteristic surface textures.
- Propose strategies to move forward in the analysis of SR in geomorphometry, toward the definition of a new paradigm in which SR is not just a set of geomorphometric derivatives but an organic branch of geomorphometric research.

The strategies are proposed with the consciousness that only the coordinated efforts of a community can overcome the challenges ahead. The design and implementation of initiatives and tools for promoting the advocated research coordination are clearly part of the current challenges in SR analysis in geomorphometry.

The discussion of the main points is accompanied by computational examples, conducted on "real" surfaces and on synthetic ones, selected and/or designed to highlight specific aspects of available algorithms. The code used to perform the experiments is based on R packages [85] and algorithms publicly available in GIS environments, to permit reproducibility and further developments. Appendix D provides more detailed information on the computations performed and related algorithms. Most computations have been performed in R using the "terra" package [86] for basic geomorphometric operations like computation of slope and the "SurfRough" package [87] for computing roughness indices. The discussion is performed mainly by analyzing raster DEMs, because geomorphometric literature and algorithms are mostly based on this most common structure. Future efforts will likely also focus on alternative representations such as 3D elevation point clouds [88,89].

In most of the examples provided, the SR is computed considering small search windows, rectangular 5×5 or circular, with a radius of 3 pixels. The choice is related to multiple reasons:

- Characteristics of the basic SR indices considered requiring a limited amount of data for their computation;
- Willingness to provide the finest possible description of local SR, still maintaining enough samples for robust estimates;
- Spatial–statistical stationarity: the bigger the search window, the higher the probability of encountering spatial statistical nonstationarity within it;
- Even considering a small search window, there are manifold aspects of SR that can be described by means of non-redundant SR indices.

2. Multiscalarity

Discussion of SR analysis must include some aspects related to spatial scale [90–93]. The concept of spatial scale, with its many facets, is central to geomorphometry and crucial when analyzing SR [1,15,16,22,39,94–96]. The relevance of spatial scale is both from the mathematical viewpoint, as in other fields concerning the analysis of spatial data, as well as from the morphogenetic interpretation. Different aspects related to spatial scale are entangled with geomorphometric analysis and algorithms. Some authors [8] prefer to distinguish between the vertical and the horizontal components of spatial scale, but the two are generally intertwined and we do not make this distinction. The aim of this section is to show the main aspects of spatial scale influencing the analysis of SR.

2.1. Generalization and Residual Topographies

A first aspect of spatial scale is the signal decomposition into different components of spatial variability, which is a key step in geomorphometric analysis. This step underlies many algorithms for the computation of basic LSPs, such as slope and curvatures [11,20,97]. When a quadratic or higher order polynomial is fitted to the data to compute a LSP such as slope, this smoothes the DEM via the polynomial. Many times, before the computation of higher order geomorphometric derivatives like curvatures, the DEM is smoothed to filter out noise and fine-scale features [97,98]. This DEM preprocessing is also referred to as DEM generalization, which is ultimately a form of smoothing. This step is required for calculating LSPs for physical-based geomorphometry and for conducting landscape segmentation [20]. In these settings, the generalization can move beyond conventional smoothing approaches based on convolutional filters. In fact, it can be conducted to fulfill contrasting requirements, such as the filtering of high frequency components except for some specific features, such as ridgelines and narrow valleys [99–101]. Accordingly, the smoothing/generalization of a DEM can be conducted via a multitude of methods, each one with its own parameters regulating the characteristics of smoothing (Figure 2). The examples (Figure 2) have been computed on a 2 m DTM derived by airborne lidar, located in the Caldera Blanca, Lanzarote (see Section 4 for further details).

The generalization/smcothing of the surface is a well-known concept in geostatistics [102] where the signal is generally decomposed in two components: the trend, representing the deterministic/structured component (the form/structure in surface metrology), and the random part, generally representing fine-scale morphology, from which the SR is often evaluated. Both components are interesting and serve different purposes. Unfortunately, the decomposition between the two is not unique and contributes to the complexity of many DEM preprocessing steps that strongly influence subsequent SR analysis. This is the case of "residual" or "relative" topographies derived by subtracting a regularized version of the terrain from the original DEM [14,103], which is a detrending procedure [102]. Under the family of "residual" topographies we find a wide range of terms such as topographic position index (TPI [104,105]), relative or local topographic position [106], and residual surface/relief [6,95,107]. Apart from very simple situations, there is not a best way to decompose the signal into two components; moreover, there is no reason to limit the decomposition to just two components. This is related in part to the complexity of surface morphology and to the specific purposes for signal decomposition, which may require specific levels of generalization/smoothing.

In addition, different approaches can be adopted to generalize the DEM (Figures 2 and 3), such as single-pass moving averages, multi-pass moving averages, moving medians, Gaussian kernels, local polynomials, or features preserving generalization. The variations between methods can be subtle, for example, the smoothing based on moving averages can use kernels that consider or ignore the central pixel in computing the mean, or can

even consider alternative kernel shapes [108]. It should be noted that depending on the purposes and the type of analysis, the generalization can be conducted either maintaining the original grid resolution [109] or changing the resolution [32]. The decomposition of the signal is relatively simple for an expedited visual analysis (Figure 3) or when the features to be highlighted have a defined range of wavelengths, such as the granulometry of a gravel riverbed. However, given the characteristics of real terrains, for quantitative analysis it may be necessary to consider different levels of generalization, which leads to multiscale approaches (see Section 2.2). The fact that a residual surface can be obtained in different ways and with different levels of smoothing (Figure 3), while providing flexibility, generates potential subjectivity in the approaches that use this kind of geomorphometric derivative, such as SR indices. It may be convenient to develop approaches that can bypass or standardize this step in SR calculations, such as in geostatistical methods using higher order increments [55,110,111].

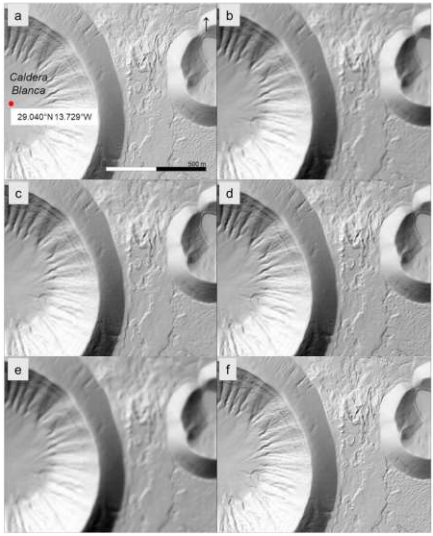

Figure 2. Hillshades of a 2 m lidar DTM (Caldera Blanca, Lanzarote, Canary Islands) and five smoothed versions, performed with different filtering approaches. (**a**) Original DTM; (**b**) moving average (3-pixel radius); (**c**) moving median (3-pixel radius); (**d**) Gaussian smoothing (11 × 11-pixel window, σ = 1 pixel); (**e**) Gaussian smoothing (11 × 11-pixel window, σ = 3 pixels); (**f**) feature-preserving smoothing. The feature-preserving smoothing was computed with WhiteboxTools 2.3.0, using the "FeaturePreservingSmoothing" function, using default parameters (11 × 11 search window, threshold set at 8, and 3 iterations).

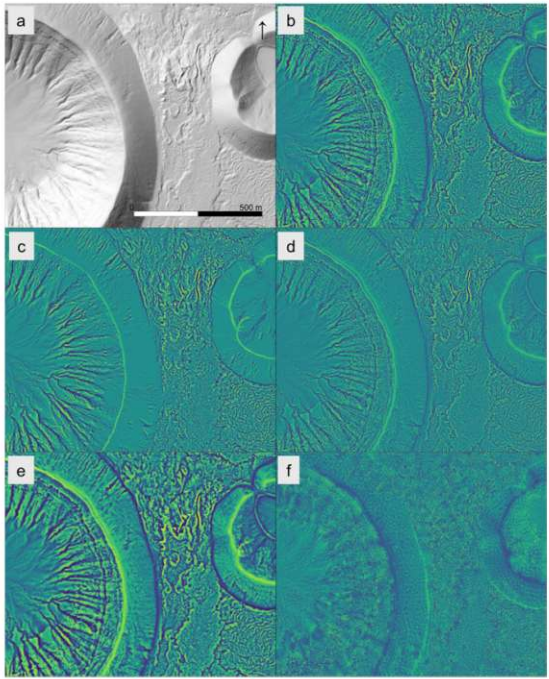

Figure 3. Derivation of residual surfaces using different smoothing approaches and different levels of smoothing, as reported in Figure 2. (**a**) DEM hillshade; (**b–f**) residual surfaces obtained with different smoothing: (**b**) moving average (3-pixel radius); (**c**) moving median (3-pixel radius); (**d**) Gaussian smoothing (11 × 11-pixel window, σ = 1 pixel); (**e**) Gaussian smoothing (11 × 11-pixel window, σ = 3 pixels); (**f**) feature-preserving smoothing. The absolute values and the spatial patterns of the residual surfaces can be quite different, influencing subsequent SR analysis.

2.2. Multiscale Approaches

The necessity to adopt multiscale approaches is related to the complexity of spatial patterns of real surfaces [1,12,48,112,113]. The spatial scale of analysis is a key issue in all those fields dealing with spatial variability, such as remote sensing, hydrogeology, pattern recognition, and spatial statistics. In geomorphometry the factor of scale has additional criticalities for two main reasons. The first one is that studied surfaces are often characterized by a hierarchy of wavelengths/ranges, and sometimes also by multifractality.

Hence, it is difficult and may be deceptive to try to define just one "right" or "best" scale of analysis. The second one is that the different scales provide different interpretations of the genetic processes and/or differently influence the modeling of surface processes like water/sediment flows.

In this context, a practical problem is that geomorphometric algorithms and related parameters, including DEM preprocessing steps such as generalization approaches [101], may act on spatial scale in different ways, influencing the computed SR indices. The key ones are represented by the pixel size, the search windows geometry (size and shape), and lag distances adopted in distance-based metrics. The pixel size generally influences both the sampling density, according to the Shannon–Nyquist sampling theorem, and the spatial support [102,114], at least when the pixel is representative of the spatial support. The last point is particularly relevant when the coarsening of resolution is performed via mean aggregation or some other form of linear operator like weighted averages or a Gaussian weighting scheme [93]. From this perspective, the smoothing performed with convolution using linear operators changes the spatial support without changing the sampling density. The search window size and shape influence the analysis in different ways depending on the specific SR index adopted. Many times, increasing the window size leads to "smoother" results, both for the averaging process inside the window and for the increased overlap between moving windows. Some SR metrics, such as the ones based on geostatistics, on spectral approaches, on local binary patterns (LBP [33,115]), and on gray levels cooccurrence matrix (GLCM [116]), are distance-dependent metrics with a direct impact on the wavelengths highlighted by the analysis. The lag distance considered in variograms or the radius considered in LBP are examples of these parameters. Another way to act on scale, in this case on the vertical dimension [8], is via thresholding/quantization, such as with the terrain texture index (TT [28,29], see Section 4.2) or with Haralick's GLCM approach. Thresholding is also linked to pattern recognition approaches such as LBP and related ST algorithms such as geomorphons [117]. Given the multitude of ways in which the user can act on the spatial scale, it is very important to keep track of all the processing steps that can influence spatial variability. The adoption of algorithms in which different processes acting on scale are intermixed, such as smoothing and selecting the search window at the same time, can make it difficult for the user to keep control of the results.

The challenges and the solutions of multiscale analysis encountered in geomorphometry, at least when dealing with raster DEMs, converge with the ones encountered in image analysis and computer vision [77,93], such as the Gaussian pyramid approach [118], wavelets analysis [119], and other smoothing approaches [109,120–122]. In the Gaussian pyramid approach, the image is iteratively smoothed and subsampled to generate a sequence of images at lower resolution that can eventually be "expanded" [118] to the original resolution via interpolation (Figure 4). Differentiating different levels of DEM smoothing (low-pass filtering) enable the isolation of specific wavelengths (band-pass filtering) (Figure 5). This is essentially the Laplacian pyramid approach [118], which can be obtained by directly applying specific filters to multilevel images such as the negative of the second derivative of the Gaussian function or the Mexican hat wavelet [120,123]. The multiscale approaches permit moving beyond a dual representation of trend and residual, and filtering out and isolating specific wavelengths. This is a key step for the multiscale analysis of SR. For a geostatistical perspective on multiscale analysis see Appendix A.

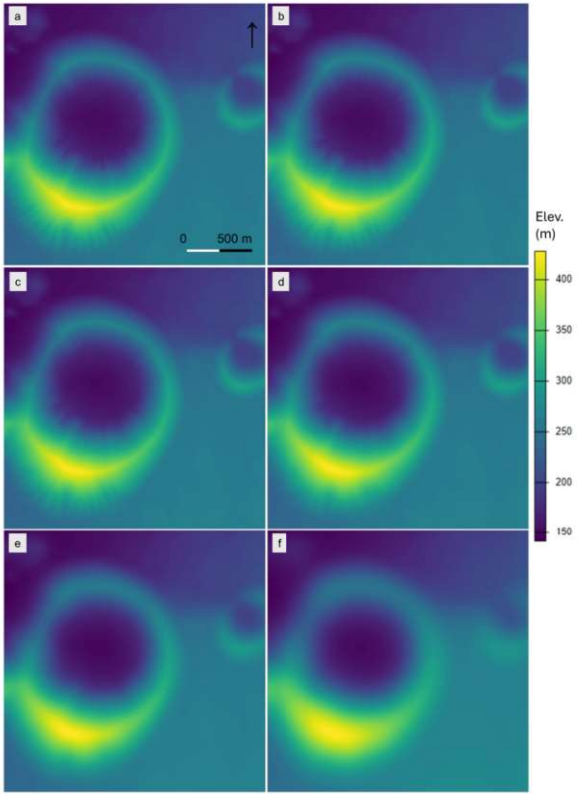

Figure 4. Application of the pyramid approach to a 2 m DTM in correspondence of the Caldera Blanca (Lanzarote) using a two-pass moving mean approach (as an approximation of Gaussian smoothing). At each level the resolution is decreased by a factor of two and then "expanded" at the original resolution via interpolation. The number of the level indicates the coarsening factor of the original resolution. (**a**) level 1; (**b**) level 2; (**c**) level 4; (**d**) level 8; (**e**) level 16; (**f**) level 32.

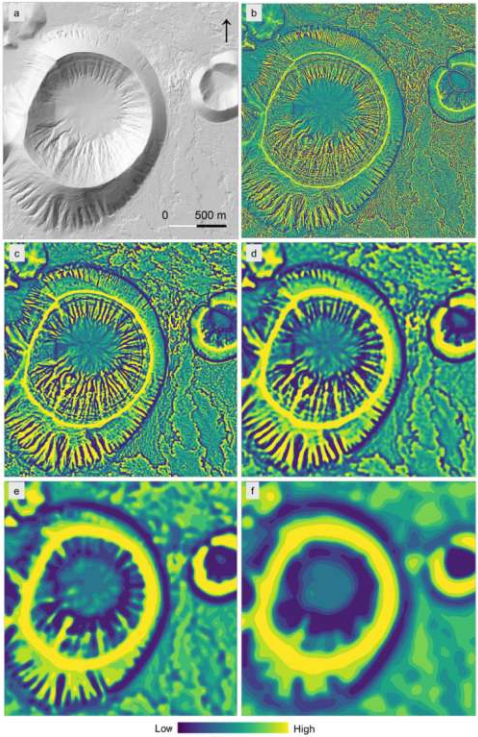

Figure 5. Differences between different levels of DEM smoothing (see Figure 4), representing a band-pass filtering (color scale histogram equalized). (**a**) DEM hillshade (2 m resolution, Caldera Blanca, Lanzarote); (**b**) DEM-Level 2; (**c**) Level 2—Level 4; (**d**) Level 4—Level 8; (**e**) Level 8—Level 16; (**f**) Level 16—Level 32. Similar results can be obtained by directly applying a Laplacian or Mexican hat filter to the multiresolution DEMs. The different levels are hence capable of highlighting specific morphologies. The first level (DEM-Lev2) highlights lava flow deposits, while Lev2-Lev4 and Lev4-Lev8 highlight erosional features along the internal and external flanks of the caldera and the lobate sedimentary deposits in the center of the caldera.

2.3. Geostatistics, Wavelets, and Surface Texture

The multiscale DEMs and residual surfaces can be used to perform a multiscale analysis of SR, convolving these with filters such as wavelets [63–65,123,124]. In this context it is worth highlighting evident analogies between wavelets and geostatistical analysis. Geostatistical ST indices can be interpreted from the perspective of band-pass filters, which highlight specific spatial patterns. A first example can be provided referring to the popular mother wavelets such as the Haar and the Mexican hat, or the wavelets obtained from the derivatives of the Gaussian function [123]. The Mexican hat is approximately the negative of the normalized second derivative of the Gaussian function, and can be computationally approximated with the difference of Gaussians (DoGs [120,123]). These filters have interesting connections with the building blocks of geostatistical bivariate estimators of spatial autocorrelation like the variogram, madogram, or MAD. These estimators are based on differences, or increments in geostatistical jargon [55,111], between pairs of samples separated by a given distance or lag and in a specific direction. We further refer to these as directional differences (DDs) and non-normalized directional derivatives (the numerator of discrete derivatives). Hence, simple differences between elevation values can be referred to as first order DDs, and these can filter out a trend of order 0, or constant trend [55]. For a gridded DEM, considering lags of one pixel and two pixels along the cardinal directions, this means, respectively, performing a convolution with the kernel $[-1; 1]$ and $[-1; 0; 1]$. For the other directions, such as the diagonals (Figure 6), to consider a lag with an integer number of pixels, the kernel is more complex. The complexity arises from the need to derive the elevation at the required lag distance via some interpolation, for example, with bilinear interpolation or other approaches [115,125,126]. The kernels $[1; -1]$ and $[-1; 0; 1]$ (Figure 7) can be seen as an approximation of the Haar wavelet and to the first derivative of the Gaussian [123].

N-S (2 px)

0	1	0
0	0	0
0	−1	0

NE-SW (2 px)

0	0.2071	0.5
−0.2071	0	0.2071
−0.5	−0.2071	0

E-W (2 px)

0	0	0
−1	0	1
0	0	0

SE-NW (2 px)

−0.5	−0.2071	0
−0.2071	0	0.2071
0	0.2071	0.5

Figure 6. Example of kernels used for computing directional differences of the first order along the cardinal and diagonal directions for square grids. Along the diagonal directions, bilinear interpolation is adopted to correct for the longer distance (see [111,125]).

A planar trend, expressed by a first order polynomial, can be filtered considering DDs of the second order, or differences of differences [55,111]. Accordingly, for a lag of one pixel, the kernel becomes $[-1; 2; -1]$, in this case approximating the shape of the Mexican hat (see also [120]). The discussion can be extended to higher orders; to filter a second order, DDs of the third order are required and the kernel for cardinal directions is $[-1; 3; -3; 1]$, again resembling the third derivative of the Gaussian, another valid

mother wavelet. The approach can go further with an increment of the fourth order, [−1; 4; −6; 4; −1], or an even higher order. The fourth order is convenient and can be quite useful in the context of physical-based geomorphometry [97,98]. Having an odd number of elements allows for computation with a 5 × 5 kernel without performing averaging processes for deriving the value on the focal pixel. It filters out a polynomial of the third order, the lowest possible order of polynomial that can computed on a 5 × 5 window; this polynomial permits to compute third order derivatives required for the analysis of the variability of curvatures [127,128]. Accordingly, it can be used to integrate SR analysis in a physical-based geomorphometry perspective. For a more in-depth mathematical analysis of the connections between geostatistical approaches and wavelets see [129,130]. Further analogies can also be found with GLCM, as well as with spectral approaches exploiting autocorrelation in the frequency domain [61,64].

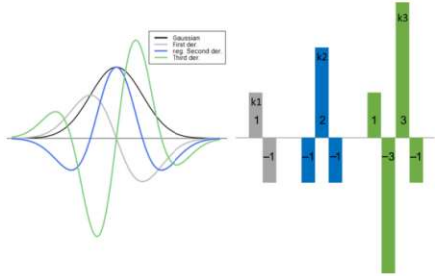

Figure 7. Analogies between DDs (increments) of the first three orders (k1–k3) used in geostatistics (**on the right**) and the shape of wavelets derived from the derivatives of the Gaussian function (**on the left**). The numbers on the vertical bars indicate the weight of the kernels.

3. Challenges

There are various efforts toward the creation of improved SR indices and the comparison of the existing ones [1,15,16,64,108,111,131,132]. However, these efforts, even if they are worth making, have several limitations, and there are open questions to be addressed. Some questions are the typical ones related to the standardization and benchmarking of metrics: according to which cost function, potentially tailored for a specific purpose, should the metrics be evaluated? With respect to which benchmark datasets? Which mathematical and statistical requirements should an SR metric fulfill? These are central questions for comparing existing SR indices and for designing new ones.

It is not easy to answer these questions, for technical reasons related to both the digital representation of surfaces and the difficulties in creating benchmark and validation datasets. In addition, it is difficult to state unequivocally what makes a metric a proper measure of SR, especially when intended in the general sense of ST. The only consensus in earth sciences [1,8,10,48] is probably that the metric should be interpretable and robust. The criteria for other properties of a roughness index are a matter of perspective. Considering the definition of SR limited to short-range spatial variability in the surface metrology sense, the characteristics of a proper index seem relatively easy to define: it should be positive, independent from the structural component of spatial variability (e.g., local slope); it should measure the variability of the surface, considering small distances between pixels; it should

use enough samples; and it should be based on a robust estimator. But what about the filtering of curvature? Should a smooth local curvature be filtered out [28,132]? And what is the threshold for defining a curved surface as smooth? This can be highly dependent on the target of the analysis and on the threshold set for defining a surface as smooth (see Section 4.3). Considering the wider concept of ST, the definition of metric properties can be trickier. An SR index might not have to be positive, and a hypothetical SR index focusing on the analysis of peaks and pits could be positive with the prevalence of peaks and negative with the prevalence of pits. The point is that the properties of an SR index may be dependent on which aspect of ST is described.

3.1. Surface Digital Representation and Apparent Roughness

The method used to sample (or measure) a surface and represent it digitally influences the fidelity of spatial variability reproduction, and thus of the SR. Two key factors govern the fidelity on SR representation: (1) the spatial sampling network (density and geometry) and (2) the measurement's spatial support (size and shape). These interlinked factors impact spatial variability, both in terms of the Nyquist–Shannon sampling theorem and dispersion variance [102,114,133]. In addition, the noise in DEMs can have various sources, including sensors characteristics, interpolation procedures, and DEM preprocessing. The noise can be both spatially uncorrelated, like white noise or hot spots, but also spatially structured, such as striping or undulations. Accordingly, it might not be trivial to discriminate against the influence of noise on the computed SR indices. We assume in the following discussion that the DEMs are in ideal condition, with all the information provided is signal.

Some limitations are related to the conventional raster representation of the surface. A raster DEM is fundamentally a 2D scalar field, obtained by projecting a 3D surface onto a horizontal plane. Within the GIS community it is often interpreted as a 2.5D surface [115], where elevation is treated as a quasi-third dimension. This interpretation enables the calculation of geomorphometric derivatives like slope and curvatures using 3D surface analysis techniques, despite the DEM's inherent topological limitations [99]. A first limitation arises from the grid-based representation. Here, we assume idealized survey conditions: near-punctual spatial support and high, homogeneous sampling density. From this high-quality elevation point cloud, a conventional regularly gridded DEM is generated, assuming an ideal interpolation/aggregation procedure. The grid geometry and 2D projection inherently influence the representation of the true 3D surface's spatial variability—and thus its texture. For a DEM in a UTM-projected coordinate system with square pixels, the effective sampling density is directionally anisotropic: it is higher along the cardinal directions (N-S, E-W) and lower along the diagonals. This anisotropy must be explicitly accounted for when computing lag-dependent indices like slope, curvatures, variograms, or autocorrelation metrics, as they are sensitive to both distance and direction [125,126]. Such considerations are critical for SR computation, whether using geostatistical, spectral, or heuristic approaches such as the TRI [3,131]. The challenge is exacerbated in global DEMs [126], which typically use a regular grid expressed in geographic coordinates (latitude/longitude); accordingly, the east–west pixel spacing, when referring to projected coordinates expressed in m, changes with latitude, and will be less than the north–south spacing. This may introduce latitude-dependent distortion in both sampling geometry and spatial support, necessitating additional corrections for consistent spatial analysis.

Another limitation stems from representing solid-earth or planetary surface morphology as seen "from above". This approach captures only an apparent roughness, not the intrinsic roughness of the true 3D surface [134]. The original 3D morphology is irrecoverably lost (Figure 8), unless restrictive assumptions about the surface are imposed [135]. While the 2D gridded DEM presents spatially homogeneous support, the true 3D spatial

support varies with local SR and slope. Similarly, the effective 2D sampling density is distorted in relation to the 3D SR. Given this biased representation, one might question the value of refining roughness metrics further. However, for many applications, particularly those focused on landscape interpretation or terrain segmentation, this apparent roughness suffices. Such tasks aim to replicate human visual perception of terrain when viewed from above, rather than quantifying true 3D surface properties. Also, for supervised learning approaches such as landslide susceptibility models at regional scale, this bias is not problematic. The use of an apparent roughness instead of intrinsic roughness can be more critical for modeling surface processes including the flow of water or wind. For specific purposes like the geomechanical characterization of rock masses, the analysis should be conducted on a different typology of projection or directly on elevation point clouds, provided that the survey is conducted from a convenient perspective [48,88,89,136,137].

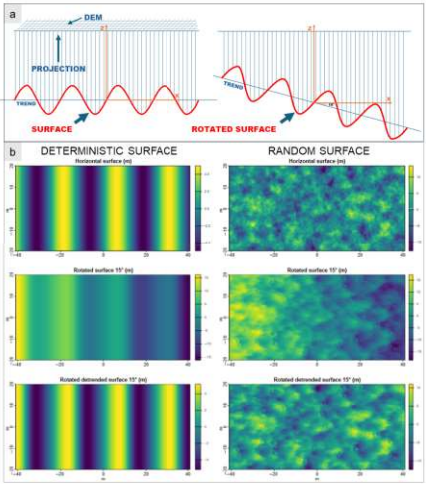

Figure 8. Impact of DEM representation on roughness considering 3D synthetic surfaces tilted to 15° with respect to the horizontal plane. (**a**) Sketch mimicking the raster representation of a 3D surface with different inclinations of the reference plane (trend); (**b**) impact of rotation on synthetic DEMs. Both the analytic (**left**) as well as the random surface (**right**), generated via geostatistical sequential Gaussian simulation, show that the SR is perceived differently when seen from above. The distortion with respect to the 3D unrotated surface is manifested with the introduction of apparent asymmetries and anisotropies.

The fact that SR is highly sensitive on the typology and quality of the digital representation of surface morphology also raises relevant considerations for the practical adoption of SR metrics for multitemporal monitoring, such as for studying the evolution of geomorphic processes related to deposition and sedimentation [6,7,14,138]. In these

settings, it is not uncommon to deal with datasets characterized by different qualities, sensing approaches, including lidar or photogrammetry, and even representation, such as raster DEMs or point clouds. Accordingly, it is fundamental to harmonize the heterogenous information available to permit a multitemporal analysis of SR.

3.2. Benchmark Data

The texture of a surface or of an image is a perceptive property [139], implying some observer subjectivity, including the scale of observation, and whether we use visual or tactile senses. For visual observers, the characteristics of the light source influence the textures highlighted, as well as scale and directional selective filters. Subjectivity also arises from human visual perception [92]. The interpretations of individuals asked to segment a hillshade or residual topography based on SR would likely differ, except in cases of very simple topographies with clearly distinct domains (Figure 9). Real terrains are often characterized by complex intermixed spatial patterns (see also Appendix B), which creates many difficulties in implementing benchmarking/references datasets such as labeled subdomains with distinctive SR.

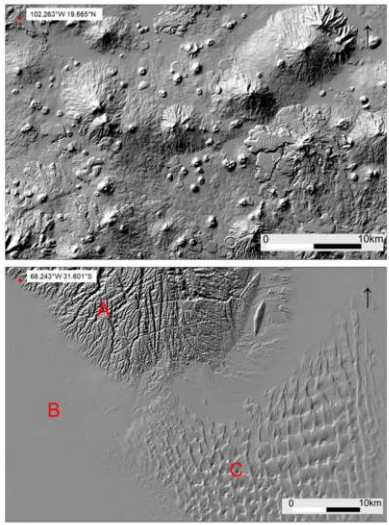

Figure 9. Hillshades from Copernicus DEM (UTM re-projected, 30 m resolution). (**Top**): Michoacán State, Mexico; (**Bottom**): San Juan province, Argentina. In San Juan, (at least) three main domains of surface texture are evident (letters A, B, C). In the case of the Michoacán volcanic area, it is not easy to decide how to visually segment the landscape according to surface texture.

The creation of benchmark datasets could be based on the approaches adopted in surface metrology and image texture analysis. In surface metrology, the surfaces often have rhythmic spatial structures, and textures are relatively simple in terms of spatial patterns. In addition, the morphogenesis of these patterns is well-known and is related to the production process and refinement procedures (e.g., milling, grinding, etc.). The standard physical specimens used in surface roughness comparators, in relation to standards such as ASME B46.1-2019 [82], present relatively simple spatial patterns for a limited range of scales (e.g., Figure 4 in [140]). A similar setting is encountered in the context of image analysis and pattern recognition. Here the textures analyzed have often repetitive patterns, and different degrees in complexity depending on the typology of represented subject (Figure 10, tiles downloaded from [141]). Generally, the higher complexity of these image textures is associated with natural surfaces, like wood or clouds in the sky. A widely used benchmark set of image textures is represented in the Brodatz collection [139], used for testing ground-breaking algorithms such as Local Binary Patterns, wavelets analysis, or conventional approaches based on fractal analysis [115,142–144].

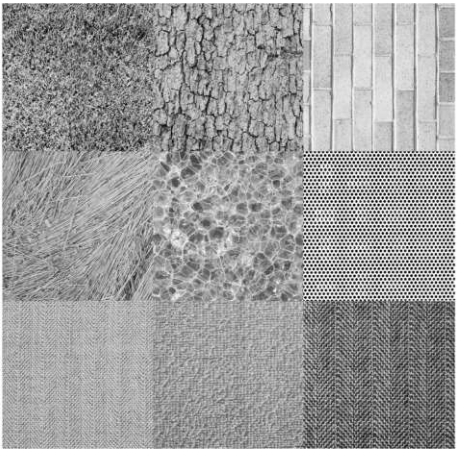

Figure 10. Example of image textures (512 × 512 pixels [141]) derived from the Brodatz collection commonly used for benchmarking purposes in computer vision. The absolute scale of the textures is not reported in these contexts, the focus being only on the spatial patterns relative to the extent expressed in pixels.

An example of a mosaic of terrain textures is presented in Figure 11, based on a lidar-derived DTM, with a resolution of 2 m and an extent of 256 × 256 pixels (for other examples, see Appendix C). We selected a resolution of 2 m because it provides good quality and filters out artifacts evident at 1 m resolution (e.g., striping). The smaller images compared to the Brodatz collection [139] cover relatively homogenous areas. Figure 11

shows the hillshade of the example terrains to visually highlight the analogies with the Brodatz collection, but actual SR analysis would use the DEMs. Datasets like this can be quite useful for benchmarking purposes but are far from exhaustive. Even the additional collection of tiles provided (Appendix C) covers only a tiny subset of textures. Their spatial–statistical characteristics could be suboptimal for benchmarking purposes; for example, in Figure 11b, patterns related to rockfall deposits are "contaminated" by the small artificial lake in the SW corner and the smooth terrain in the SE corner of the image.

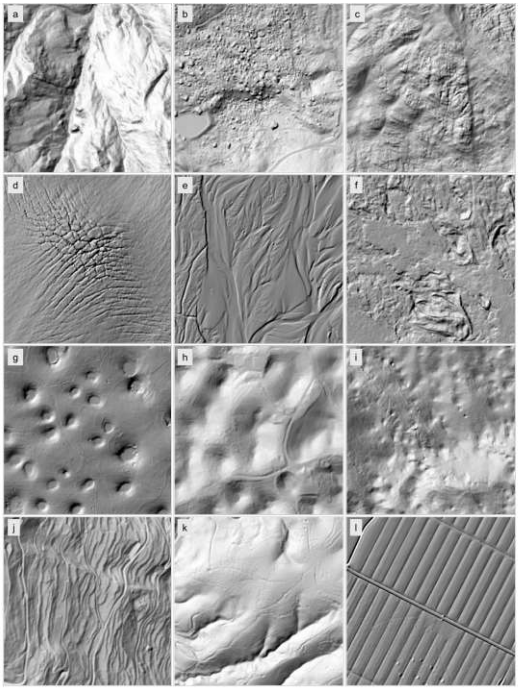

Figure 11. Example of a mosaic of terrain textures tiles (512 m × 512 m), represented with a hillshade derived from 2 m resolution DTMs (256 × 256 pixels), compared to the Brodatz collection. (**a**) Alpine valleys; (**b**) rock fall deposits; (**c**) fractured rocky outcrops; (**d**) fractures in an alpine glacier; (**e**) active riverbed; (**f**) lava deposits; (**g–i**) karst, dolines fields; (**j**) terraced landscape; (**k**) karst, fluvial incisions, and first world war trenches; (**l**) cultivated fields.

The earth and planetary morphologies have special characteristics, such as the presence of coalescent multiscale structures, sometimes exhibiting a multifractal behavior, and are most of the time nonstationary in the spatial–statistical sense (Appendix B, Figure A2). One specific aspect of nonstationarity is represented by spatial discontinuity, manifested by abrupt morphological transitions like punctual features, lineaments, and sharp variations from one textural domain to another. The presence of discontinuities in surface morphology has a special significance for both interpretation and the impact on the calculation of SR indices, especially when using nonrobust estimators.

3.3. The Atlas of Surface Textures

Given the wide range of terrestrial and extraterrestrial terrain patterns, it would be useful to implement a geodatabase atlas of surface textures (AST), consisting of DEM tiles, that represents a wide set of distinctive surface textures. The AST would permit isolating specific spatial patterns, to eventually be mimicked by synthetic DEMs and used for designing specific SR indices. This geodatabase could be particularly useful for benchmarking, testing, and training machine learning approaches. The design and implementation of an AST present a series of practical and theoretical issues. We limit discussion to conventional raster DEMs, currently by far the most widely used representation.

The scale of analysis must be carefully considered in the design of an AST. Different processes act at different scales to generate specific patterns, even if some patterns may exhibit self-similar or self-affine behavior. The AST should contain collections of different resolution surfaces, with an extent large enough to statistically describe the landscape patterns. Describing complex multiscale patterns may require larger extents compared to the 256 × 256 pixel size in Figure 11. For instance, the examples in Figure A2 cover a diverse range of scales and extents in number of pixels (Figure 12). The AST should have a variety of extents and resolutions.

The range of resolutions to consider is a difficult choice, even if the choice is partly related to available sources of data with open licenses. A possible solution is to consider the characteristics of commonly available DEMs and the main typologies of applications. Resolutions of 1–5 cm could be useful for micro-morphological studies focusing on river-bed morphology, fracture analysis, or karstic morphological features like karrens. Resolutions between 0.5 m and 2 m, available from various national and regional repositories around the globe, can be tailored to many geoenvironmental applications from local to country scales. Lower resolutions, typically used for global DEMs (e.g., up to 30 m of pixel size or even larger), can be useful to describe terrain patterns at larger wavelengths or peculiar patterns that are not described by available higher resolution data. However, it should be considered that with 30 m DEMs, such as the Copernicus DEM [145,146], fine-scale features are filtered out (Figure 13) according to the Nyquist–Shannon theorem. This occurs irrespective of other quality concerns associated with global DEMs [147].

A second issue is related to the statistical representativeness and characteristics of represented textures. Which, if any, spatial–statistical requirements should a DEM candidate have to be considered representative? We could expect that a texture tile should be representative of a characteristic pattern, assessed by some criteria of homogeneity, but it is not easy to define criteria (e.g., [148,149]). Should homogeneity be assessed visually by analyzing the hillshade or residual surface, or quantified with some spatial–statistical index? And how to handle hierarchies and/or mixtures of spatial patterns? What quality should the source DEMs have, and what procedures would guarantee the quality of DEMs? Which protocols could detect artifacts and spurious spatial patterns in the DEMs?

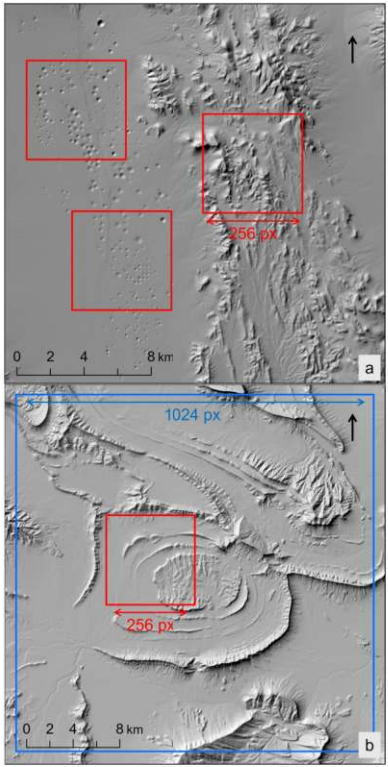

Figure 12. Characteristic textures visible from 30 m DEMs (UTM re-projected Copernicus DEM): (**a**) Nuclear sinkholes (NV, USA); (**b**) folded strata (Monterrey, Nuevo León, state, Mexico). Depending on the range of different textures, the number of required pixels per tile to represent "characteristic" textures can change. In (**a**) 256 pixels can be enough; in (**b**) much larger tiles are required.

Practical aspects considered in the design of an AST include smart structuring, with categorization of surface textures and the possibility to integrate new textures. Temporal dimensions should reflect a surface that is dynamic, and new technologies will allow for higher-quality terrain representation. The AST should contain a large sample of real terrains,

and also contain a set of synthetic surfaces which permit control of surface properties, isolate specific aspects, and mimic the impact of different digital representations. The inclusion of synthetic surfaces in the AST can be more straightforward than for real surfaces, but the generation of synthetic surfaces has many degrees of freedom. Indeed, the surfaces can be generated by both numerical and physical methods (e.g., [55,150–154]). Numerical approaches include analytic surfaces, stochastic surfaces, and AI generation. The surfaces can be produced by physical means, such as the creation in concrete or asphalt, 3D printing, or other manufacturing approaches (e.g., [150]).

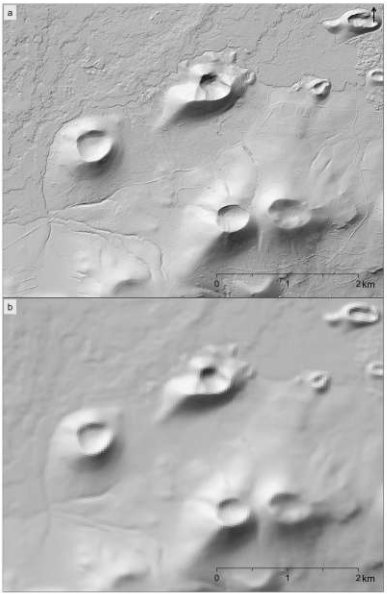

Figure 13. Hillshade of lidar DTMs at different resolutions for an area in Lanzarote. **(a)** 2 m; **(b)** 30 m, derived by means of pixel aggregation (average of 15 × 15 pixels at 2 m resolution). The filtering of fine-scale detail can be critical for multiscale SR analysis.

As further discussed in Appendix C, the design and implementation of the AST is a complex task, which requires much testing in addition to theoretical design. The examples of collections of tiles we provide with the paper are a tiny subset of what a first prototype version of the AST could be. One of the great challenges underlying the implementation of the AST is to effectively promote a collaborative shaping effort.

4. Revisiting Basic SR Indices

The set of widely adopted and readily available algorithms for computing roughness indices in GISs (ArcGIS, Grass, Microdem, Saga and Whitebox) and programming languages (Python and R) is reported in Table 1, with further details reported in Appendix D. More complex approaches adopting geostatistical, spectral, fractal, and other methodologies for the analysis of surface texture (e.g., [1,33,58,61,63,64,124,125]) are not included. End users prefer adopting compact SR indices, requiring few or no decisions regarding calculation parameters. Sometimes, this desire for simplicity leads to the misuse of available indices, such as the Topographic Ruggedness Index (TRI) [3,39], which from a geomorphological perspective measures neither fine-grain texture ("roughness") nor broader-scale morphology ("ruggedness"). In fact, the TRI in most terrain conditions is practically a proxy of slope [131], at least when applied directly to a DEM and not a residual surface.

Most reported SR indices, even if developed from different perspectives, are relatively simple measures of ST. These indices catch overall local spatial variability at a specific scale or within a limited range of scales determined by the size of search window and DEM resolution. The capabilities of these indices can be extended, as with any geomorphometric derivative, performing their calculation in a multiscale fashion, such as with a Gaussian pyramid approach (Section 2.2) or adopting multilevel smoothing [15,94,95,109]. However, for a given scale, these indices have limited capability to describe specific aspects of ST and hence to be adapted to the different purposes that may underlay a geomorphometric characterization. Table 1 includes the "terrain texture" (TT) index used by Iwahashi and Pike [28,29] and implemented in Saga GIS [155], given its relevance for segmenting the landscape and its potential to describe specific aspects of surface texture, as discussed in Section 4.2. The last indices included are the radial roughness index (RRI, [131]), which overcomes the main drawbacks of the TRI, and a simplified geostatistical approach based on the MAD estimator [111,125] (see Appendix A), adaptable to detect specific aspects of surface texture.

The simplified geostatistical SR indices represent a valid, compact, and robust alternative to conventional basic indices. The methodology used to develop these indices, including the RRI, exemplifies how a robust theoretical framework—such as geostatistics—can be used to synthesize simple yet informative surface topography indices while minimizing the number of user-defined parameters. The simplified geostatistics-based indices considered in Table 1 are capable of considering specific lag distances and directions, permitting them to detect different aspects of ST, such as anisotropy in SR [111].

Table 1. Basic surface roughness indices widely adopted and some recent improvements (Appendix D for more details).

Roughness Index	Acronym Used in the Paper	Description	Key References
Topographic ruggedness index	TRI	Radial variability of elevation respect to a central pixel, computed on a 3×3 rectangular window. Most often computed as the mean of the absolute differences in elevation between the eight external pixels and the central one. Remark: proxy of slope if not applied to a residual surface. Units: m.	[3,39,131]

Table 1. *Cont.*

Roughness Index	Acronym Used in the Paper	Description	Key References
Standard deviation of residual surface	STDres	Standard deviation of residual elevation computed on a moving window. Variability computed in all directions and for different lag distances. It is dependent on the approach adopted for deriving the residual surface. Units: m.	[6,104,108,156]
Standard deviation of slope	STDslope	Standard deviation of slope computed on a moving window. The same approach can be extended to other geomorphometric derivatives (e.g., curvatures [15]). Units: % or °, depending on the units used for slope.	[7,15]
Surface area ratio	SA	Surface area methods based on the departure of the topographic surface from a smooth "ideal" surface. Metric derived computing the ratio between the "true" surface and the "ideal" one in a local window. The version of Du Preez corrects for the dependence on slope. Units: dimensionless.	[48,50,108,157]
Normal vectors dispersion (also known as vector ruggedness measure, VRM)	NVD	Based on circular statistics, computes the dispersion of normal vectors to the surface in a moving window. Compound measure of roughness highlighting morphological features at multiple wavelengths. Enhances elongated and linear features. The method can also be extended to the analysis of roughness anisotropy. Units: dimensionless.	[13,48,108,158]
Radial roughness index	RRI	The RRI improves the TRI, reducing the dependence on slope using second order differences and correcting for the different distances between cardinal and diagonal directions. Larger kernel (5 × 5) with respect to the TRI. Units: m.	[131]
Simplified geostatistical approach based on MAD of DDs of order 2	MAD_{k2}	Geostatistical-based SR indices using second order DDs. Applied directly to a DEM without detrending. Short-range roughness indices (max lag distance 2 pixels). In addition to omnidirectional roughness (units: m), also computes roughness anisotropy (strength and direction).	[111]
Terrain texture	TT	Number of pits and peaks inside a moving window (originally 10 × 10), calculated from a residual surface, derived via median smoothing (originally with a moving window 3 × 3). Depending on the implementation (e.g., Saga) a threshold can be defined for defining peaks and pits. Units: %.	[28,29]

To provide an overview of the information extracted by these indices, we consider an emblematic surface (Figure 14) in a portion of Lanzarote Island (Canary Islands, Spain). The "Caldera Blanca" is surrounded by lava flows and to a minor extent by sedimentary deposits [159]. The SR indices and relative statistics are computed for the overall domain

of Figure 15; smaller maps for significant subzones (spots 1–3) enhance details. The 2 m DTM has been derived by the interpolation of an airborne lidar point cloud (density at least 5 pts/m^2), publicly available from the Spanish "Instituto Geográfico Nacional" (Lidar 3rd coverage 2022–2025, downloaded from [160]). The DTM (available in [161], including also RGB imagery) was specifically selected both for the quality of the data and, in particular, the absence of unwanted artifacts.

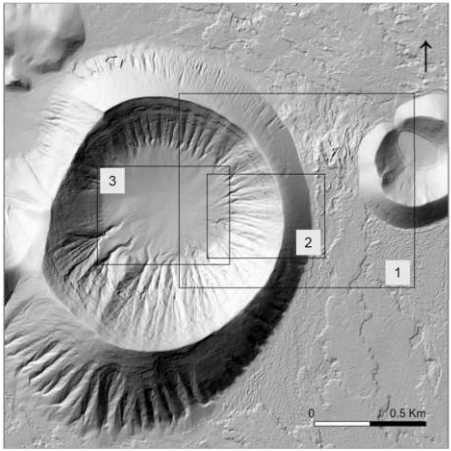

Figure 14. Hillshade of the test DTM used for describing basic SR indices, corresponding to Caldera Blanca, Lanzarote Island (numbered black boxes represent specific spots displayed in subsequent figures). The statistics of the computed SR indices are referred to the full domain.

The terrain selected highlights the key characteristics and limitations of ST indices based on the following morphological features: sharp variations in roughness alternating with smooth variations; multiscale morphological features; anisotropic and curvilinear features; features with high curvature but smooth from the perspective of fine-grain roughness; areas with sharp variations in slope; presence of "outliers" such as local bumps and lineaments. The analysis of the indices is presented with maps and a Pearson correlation analysis between indices. Unless otherwise specified, the color scale is based on a histogram equalized viridis color spectrum [162], with quantile classification to focus on spatial patterns of the histogram equalized classes more than absolute values. Statistical distribution of SR indices, such as skewness and kurtosis, can influence subsequent processing of computed values, for example, when used in unsupervised or supervised machine learning approaches. The statistical characteristics and the measurement units of the returned SR indices could be another factor to consider for specific applications. The distortions of statistical distributions can be partially mitigated with data transformations approaches, such as logarithmic and Box–Cox transformations. However, data transfor-

mation approaches have their own complexities and subjective choices. Accordingly, SR indices less prone to produce statistical distribution with heavy tails should be preferred.

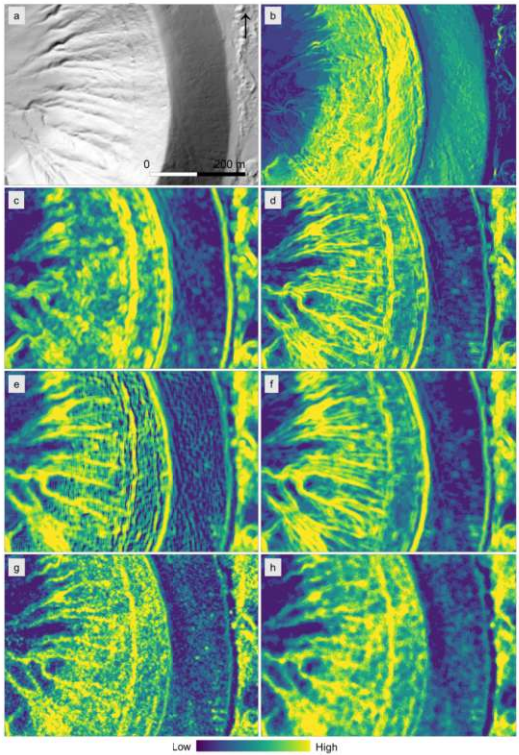

Figure 15. Popular omnidirectional roughness indices and new simplified approaches based on geostatistics (RRI and MAD_{k2}). Particular of spot 2 (Figure 14): (**a**) hillshade; (**b**) slope (%); (**c**) STDslope (%); (**d**) STDres (m), with residual computed via local first order polynomial (MultiscaleDTM R package); (**e**) SA (MultiscaleDTM R package); (**f**) NVD (also known as VRM); (**g**) RRI (m), radial roughness index; (**h**) omnidirectional MAD_{k2} (m), computed for a lag of 1 pixel. Color scales histogram equalized with quantiles classification.

4.1. Basic Surface Roughness Indices

In this subsection we introduce and compare popular basic SR indices (Table 1), highlighting their conceptual framework and their main characteristics. In the comparison we do not include the popular TRI, given the underlying drawbacks; instead, we include its improved version, the RRI [131]. These indices provide some measure of the local overall surface spatial variability, filtering out the local slope, in the sense that a steep flat plane should return an SR index of zero and not a high value [108]. Despite various heuristic or theoretical approaches, the different basic SR indices are correlated, especially when considering small search windows. Indeed, the general patterns (Figure 15) of these SR indices are similar, as also confirmed by the linear correlation values (Figure 16). However, there are relevant differences, especially when looking at the details, which often matter more than the general trend. These differences are related to the different robustness of estimators and to the different designs of the SR indices, which tend to highlight selectively specific morphological features.

Figure 16. Linear correlation between selected omnidirectional roughness indices. STDslope: standard deviation of slope; SA: area-based method; STDres: standard deviation of residual surface, with trend computed with a local polynomial of order 1; NVD: normal vector dispersion; RRI: radial roughness index; MADk2omni: omnidirectional MAD with DDs of order 2 and a lag of 1 pixel.

4.1.1. Spatial–Statistical Variability Estimators

The different robustness of the estimators to outliers and nonstationarity [55,125] used in SR indices contributes significantly to the differences observed. The discussion on robustness permits the introduction of two very simple yet effective SR indices: the standard deviation of residual surface (STDres, Figure 15d) and the standard deviation of slope (STDslope, Figure 15c). The underlying principle—evaluating the dispersion of selected LSPs in a search window—can be applied to other LSPs as well [15]. The way in which LSPs are calculated impacts the computation of SR, in addition to the selection of the search window size. As reported in Section 2.1, there can be relevant differences between the derived residual surfaces, in relation to the different smoothing approaches and levels. There may also be differences for slope between algorithms, especially when kernels larger than 3×3 pixels are used [98]. In the example of Figure 15, slope has been calculated within the R "terra" package [86] and the residual surface using the "adjusted"

version of the MultiscaleDTM package [108], which use a first order polynomial (plane) to compute the local trend. Both STDslope and STDres, being based on the mean estimator and squared differences, are inherently nonrobust, and hence highly sensitive to data contamination and nonstationarity. Practically all the reported indices, except for MAD (see Appendix A.2), are based on an averaging process, and affected by this drawback to some extent. In STDslope and STDres this is accentuated using squared differences and by the set of data pairs that are considered. To highlight this aspect, it is convenient to represent the variance in an alternative form to the conventional formulation. Considering a search window comprising n z_i pixels, the conventional formulation of the experimental variance is a linear combination of squared deviations from the mean m of the n pixels. The variance can also be defined in terms of all the combinations of squared differences between the n pixels (i.e., DDs) [102]:

$$\sigma^2 = \frac{1}{n}\sum_{i=1}^{n}(z_i - m)^2 = \frac{1}{2n^2}\sum_{i=1}^{n}\sum_{j=1}^{n}\left(z_i - z_j\right)^2 \quad (1)$$

In the case of STDres the pixel values are residual elevations and in the case of STDslope these are slopes [7]. This representation is convenient because it highlights why these indices provide a bulk evaluation of SR and are very sensitive to noise and nonstationarity. These consider different lag distances and directions or, in other terms, consider the set of all DDs that can be found in the search neighborhood (Figure 17a). This implies that these SR metrics can activate multiple wavelengths in multiple directions. In addition, one anomalous pixel (e.g., a spike) will affect many DDs, amplifying its effect. In the case of STDslope, the index is a kind of hybrid between an omnidirectional and directional one, given that the slope is computed only in the direction of the gradient. For larger windows, longer distances are considered for the DDs; hence the impact of the window size on the computed indices is dependent on the spatial autocorrelation structure. Regarding the shape of the search window, considering a grid with square pixels, using a square search window, the longest lags considered will be along the diagonals, and with a circular window, the longest lags considered will be along the cardinal directions, leading to potentially slightly different results in case of anisotropic features. Given these characteristics it is not surprising that these indices are not robust to sharp variations in surface morphology and the presence of outliers [16,125].

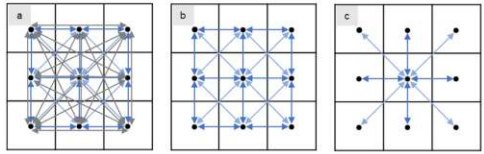

Figure 17. Sketch showing different sets of directional differences (DDs) inside the considered kernel/search window define different roughness estimators. The standard deviation of residual surface or of slope considers all possible combinations of DDs in the kernel (**a**). A geostatistical estimator, such as the variogram, madogram, or MAD, consider specific lag distances (**b**) or even specific directions. The TRI considers only the differences between the central pixel and its surroundings (**c**).

Indices such as STDres and STDslope can be easily improved by substituting the standard deviation with the interquartile range (IQR), which is a robust estimator of dispersion (e.g., not sensitive to outliers). Accordingly, these can be computed with standard focal operations, directly using the interquartile range as an estimator or calculating the first and

third quartile and then computing the IQR. In Figure 18, we compare the spatial patterns of the conventional STDres with a robust version based on the IQR as a measure of dispersion (IQRres), considering a circular search window with a radius of three pixels (i.e., 29 samples are used to compute IQR). The residual surface has been derived smoothing by moving averages (circular window, radius 3 pixels). The robust version provides a less blurred representation of roughness, describing more sharply abrupt morphological transitions and reducing the areal influences of local anomalies.

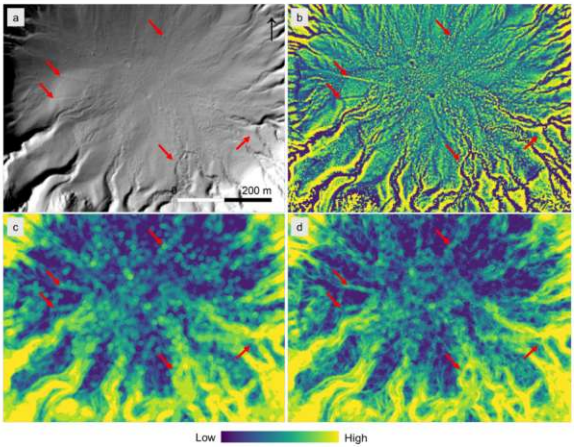

Figure 18. Interior of the Caldera Blanca (Figure 15, spot 3), comparing STDres with its robust version based on IQRres. Red arrows highlight interesting morphological features. (**a**) Hillshade; (**b**) residual surface (m), smoothing with moving mean, search radius 3 pixels; (**c**) STDres (m), search radius 3 pixels; (**d**) IQRres (m), search radius 3 pixels. The robust version produces a sharper representation of SR. Note that the bumps related to rock blocks and some unfiltered vegetation generate the spotty appearance on STDres, obliterating some sediment-flow-related patterns. High variability structures (e.g., gullies) appear enlarged in the STDres map, contributing to the blurring effect, which it is not present in IQRres. Color scale histogram equalized (quantile classification).

The alternative formulation of the variance (Equation (1)) facilitates the comparison of STDslope and STDres with other methods, such as the TRI, RRI, and geostatistical methods, which ultimately select specific sets of DDs (Figure 15b,c). Geostatistical methods are selective in lag distances and directions. The TRI and RRI consider, respectively, DDs of orders 1 and 2 between the central pixels and their neighbors [3,131]. The RRI and simplified geostatistical methods are discussed in more detail in [111,125,131] and Appendix A; see also Section 4.3 for further modifications. The RRI (Figure 15g) is an improvement over the TRI, which uses DDs of the second order to compute the average radial roughness, i.e., the variability with respect to the central pixel considering a 5×5 kernel, without needing detrending or user-defined parameters. It also corrects for the different distances between

pixels in the cardinal and diagonal directions. The geostatistical index MAD_{k2} [111] is part of a simplified geostatistical approach, designed to balance flexibility and method complexity. It is based on the MAD estimator [125] with increments of order 2, requiring only two user choices, search window size, and lag size (0.5, 1 or 2 pixels). This bypasses the many subjective choices required for derivation of the residual surface. The simplified MAD_{k2} approach provides two basic indices, short-range omnidirectional SR (Figure 15f, SR in the surface metrology sense) and two-component (strength and direction) anisotropy in short-range SR. SR anisotropy, discussed in the next section, is related to the lay in the surface metrology sense (Figure 1). Short-range DDs only consider short lag distances (e.g., max two pixels). In the example provided, for improving the comparison with the RRI and the other basic considered indices, a lag of 1 pixel and DDs of order 2 have been selected, and the metrics are computed with a circular window with a search radius of 3 pixels, permitting statistics with 29 DDs (comparable with the 25 of a rectangular 5×5 kernel) in each of the four directions considered. Given the design of geostatistics-based indices [125], the effective search radius of MAD, in terms of elevation values considered, is 4 pixels (search radius plus the lag distance). The omnidirectional roughness (Figure 15f) averages directional short-range SR in four directions/azimuths (cardinal and diagonal directions).

Even if the RRI is based on a mean estimator, it is less sensitive to anomalous local pixels found in the search window compared to STDres or STDslope. With the RRI, an anomalous pixel found in the search window is not amplified by multiple DDs affected by that pixel, if the pixel is not the central one.

The differences between the basic SR indices are not only due to estimator robustness but also to other design characteristics. STDslope provides different spatial patterns with respect to STDres in correspondence to the straight part of the gullies in the internal flanks of the Caldera Blanca (Figure 15). Along these features, the slope is predominantly constant, and consequently these features are not highlighted by STDslope, unlike STDres and other indices.

4.1.2. Heuristic Approaches

Another way to represent the overall variability of the local surface is to evaluate the ratio between the area of the actual surface with the one of an ideal smoothed reference surface [48,50,108,157], leading to the surface-area-based methods (SA, Figure 15e), sometime referred to in the ecological literature as "rugosity", another synonym of SR. The higher the ratio, the higher the SR. The way in which the "ideal" surface is computed impacts the measures of SR. The first implementations considered a flat horizontal surface, and thus depended on local slope. A more effective approach [50] considers a best fit plane to the data to filter out the effect of local slope. We tested the Du Preez algorithm as implemented in MultiscaleDTM [108]. Figure 16 shows this method as highly correlated with NVD but provides some unrealistic crenulated patterns, especially along the smooth flanks of the Caldera Blanca.

A well-known alternative approach for evaluating a measure of overall roughness is expressed by the dispersion of normal vectors (NVD) to the surface [4,13,158,163]. This is a quite effective method, despite some dependence on local slope [111]. The main idea is that higher NVD occurs in rougher terrain. NVD is popularly known as the vector ruggedness measure (VRM) even if, in the geomorphological sense, it represents roughness or ruggedness depending on the kernel size. The dispersion or circular variance can be computed considering eigenvalues or the resultant length of the mean vector [13,158]. NVD is implemented, with some variation, in most software, and can be adapted to evaluate the directionality/anisotropy in roughness/fabric [66,158]. In addition, alternative versions such as the "spherical standard deviation of normals" are available in Whitebox [22]. This

modification, useful in the context of multiscale analysis, is a normalized version that filters out unwanted details for the specific scale selected. Even if NVD is a kind of bulk evaluation of roughness, it is highly sensitive to anisotropic features and tends to provide high values even when these features are smooth at fine-scale [111]. Examples of these features are the ridges of the calderas, the gullies, and the change in slope at the external flanks of the caldera (Figure 15f). The correlation with SA (Figure 16) is very high in this setting, but NVD does not present the artifacts seen in SA (Figure 15e). This index is affected by nonstationarity and outliers.

4.1.3. Basic Surface Roughness Indices: Practical Guidelines

Although the selection of an SR index is often application-dependent, general guidelines can be formulated. Most of the basic SR indices considered, except for MAD_{k2}, exhibit high dependency on outliers and nonstationarity. This dependency can lead to a blurred representation of roughness, due to the creation of a buffer around features with a high spatial variability or corresponding to abrupt transitions from different textural domains. Furthermore, the indices based on nonrobust estimators also have the secondary effect of shrinking areas of low roughness when surrounded by more rugged terrain. Accordingly, the use of indices based on nonrobust estimators can be an issue, especially when analyzing high resolution DEMs and/or DEMs with the presence of artifacts. The primary justification for using a nonrobust estimator would be when the specific goal of the analysis is to emphasize such artifacts or hotspots, as in DEM quality assessment.

All the basics indices discussed, except for the RRI and MAD_{k2}, compute SR while integrating multiple lag distances, and hence are not distance-selective. They provide an overall measure of SR, capturing morphological variability across a range of scales up to the size of the search window. As a result, a larger window incorporates the influence of larger-scale features. In contrast, approaches capable of selecting specific lags, such as MAD_{k2} and RRI, function differently. For these, increasing the search window size does not alter the target lag distance itself, but rather expands the spatial extent used in the estimation. This predictable and scale-invariant behavior is generally preferable, particularly when employed within multiscale analysis frameworks (Section 4.4).

Based on the above considerations, we propose the following guidelines in relation to the basic SR indices discussed:

- MAD_{k2} should be preferred for a robust evaluation of short-range omnidirectional roughness, given its robustness and the possibility to derive other SR indices such as SR anisotropy (Section 4.2). It is particularly well suited to perform multiscale analysis.
- The RRI can be an alternative whenever the radial evaluation of roughness is meaningful for the application at hand (see also Section 4.3). This is often the case in ecological applications, in which the interest is in the terrain roughness as perceived from a central point.
- NVD can be useful to highlight features with high curvature, such as ridges, gullies, scarp margins, changes in slope, and similar morphological features. NVD characterizes multiple spatial scales, with the largest scale limited by the window size. Therefore, one should evaluate whether the modified version based on the spherical standard deviation of normals [22] should be preferred for the task at hand.
- STDslope can provide complementary information to other indices, though its results can be visually counterintuitive. It is useful in specific contexts, such as the analysis of surface flow processes.
- STDres provides a basic, highly interpretable overall measure of surface variability [6,139]. A key consideration is that the multitude of methods for deriving the residual surface presents both opportunities for customization and challenges for

standardization. Moreover, once the residual surface is computed more complex geostatistical and spectral approaches can be adopted.

- STDslope and STDres, and analogous indices based on STD of LSPs, are nonrobust. These indices can be made robust considering the IQR instead of the STD. We suggest using IQRslope and IQRres as better alternatives.
- We do not recommend SA given its tendency to present artifacts and the similar information provided to NVD.

4.2. Detecting Specific Aspects of ST

The correlation between SR indices decreases when specific aspects of ST are described, even when considering small search windows (Figures 19 and 20). One of these is represented by the anisotropy in SR [11,12,30,59,125,164–168], i.e., when the terrain is characterized by preferential orientation. Looking at SR as an impedance factor, short-range SR can be seen as a tensorial property, changing with direction in analogy to hydraulic conductivity. The simplified approach based on MAD and MAD_{k2} describes this fact, and could be exploited for the analysis and modeling of surface flow processes (e.g., [169]). Another strategy to catch specific aspects of ST is based on thresholding approaches, like in the TT index [28,29], which essentially acts on the amplitude of morphological features that are considered in SR computation.

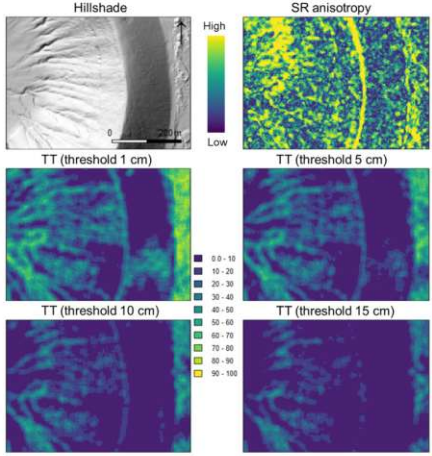

Figure 19. SR anisotropy strength based on MAD_{k2} for a lag of one pixel (0 isotropic, 1 maximum anisotropy) and terrain texture (TT, % of pixel that are a pike or a pit in the search neighborhood) of Iwahashi and Pike, considering four different thresholds for classifying a pixels as a pike/pit (i.e., if the absolute residual elevation is below the threshold it is considered flat). Color scale histogram equalized for SR anisotropy and equal interval classification for TT.

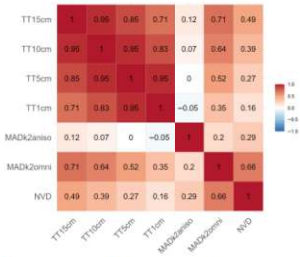

Figure 20. Correlation between selected SR indices. TT: terrain texture [28]; MADk2aniso: anisotropy strength in short-range roughness; MADk2omni: omnidirectional short-range roughness; NVD: normal vector dispersion.

TT is another bulk SR metric that has some popularity, and it is based on a different perspective in describing ST. It looks at the number of bumps, represented by pits and peaks, present in the search window. It is based on three main steps: (1) calculation of a residual surface via median smoothing (3 × 3 window in the original papers); (2) classification of negative pixels as a pit and positive ones as a peak; and (3) computing the percentage of pixels classified as peaks or pits within the search window. Step 2 can be viewed as a discretization/quantization process or a binary classification, analogous to image texture approaches such as LBP [33,115] and GLCM [116]. TT depends on the calculation of residual surface and threshold set for classifying a pixel as a pit/peak. The threshold in the absolute value of the residual surface acts on the vertical scale and the amplitude of morphological features is considered. Setting tiny thresholds implies that the texture is computed independently from the amplitude of local morphological features. In Figure 19, the index has been calculated using the SAGA (tool "Terrain Surface Texture, SAGA version 9.3) considering a 5 × 5 search window, to be compatible with preceding calculated indices, and selecting different thresholds (1, 5, 10 and 15 cm) for highlighting the impact of the threshold. By increasing the threshold, the patterns more closely resemble those computed with basic SR indices (Figures 15 and 20). The correlation between TT computed at the lowest and highest thresholds (1 cm and 15 cm) is relatively low, indicating that changing the threshold provides different information. The TT can be modified in many other ways, both regarding the computation of residual surface as well the way pixels are classified. If it is useful for the analysis, one can classify pixels as pits and peaks, setting the threshold between a minimum and maximum difference, isolating specific amplitudes of roughness. But higher flexibility also means higher subjectivity in choices and difficulties in comparing different studies.

SR indices derived by the GLCM method relate to a fundamental approach in image texture algorithms for pattern recognition and remote sensing [116,144,170]. The application of this method in geomorphometry is not particularly popular, probably because some computed indices are not readily interpretable from a geomorphometric perspective, and some are redundant. Moreover, results strongly depend on the quantization approach adopted before computing transition probabilities. The approach has several analogies with geostatistical and spectral methods, given that all are essentially based on autocorrelation measures or transition frequencies between neighboring pixels [144]. To be used for ST analysis, the algorithm should be computed on a residual surface, which is subsequently

quantized in a set of integer levels, generally 16 or 32. The quantization in integer levels may be conducted with different approaches, such as equal intervals in the range of data or quantile classification.

The GLCM analysis presented in Figure 21, conducted with the implementation in the R (package GLCMTextures [171]), evaluates the main GLCM indices for specific combinations of pixels. To compare the results with the previously calculated SR indices, the nearest neighbor pixels in the cardinal and diagonal directions have been considered and a 5×5 window selected. The residual surface has been derived with moving means with a circular window with a radius of 3 pixels. The quantization has been performed in 16 classes using quantile classification. The same residual surface is also used to compute SR indices using MAD [125], with DDs of order 1. Omnidirectional SR and SR anisotropy have been computed with a lag of 1 pixel and a circular window with a radius of 3 pixels. In addition, another geostatistics-based SR index has been computed, the relative roughness [30], which is defined in this case as the ratio between the omnidirectional SR computed for a lag of 1 pixel and the average omnidirectional SR computed considering multiple lag distances, in this case 1, 2 and 4 pixels. Relative roughness provides information as to what extent the overall terrain variability is expressed at short-range. High values of relative roughness are generally found on scree slopes, because the terrain is rough at short-range and quite smooth at long-range. It can be seen (Figures 21 and 22) that some GLCM-derived indices are correlated and some are not easily interpretable from the geomorphometric perspective, such as the GLCM correlation. The more correlated GLCM parameters are the group contrast, dissimilarity, and variance and the group homogeneity, entropy, and angular second moment (ASM). Indices variance, entropy, and correlation can be considered to provide non-redundant information. The GLCM_mean is essentially a smoothed version of the original residual surface and can be derived by much simpler methods. There are some analogies (Figure 23) between the three selected GLCM patterns and the considered geostatistics-based ST indices, with a particularly high correlation (Figure 24) between omnidirectional SR and variance.

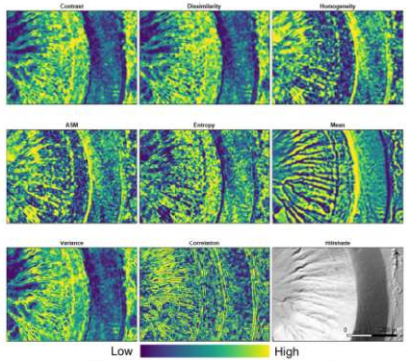

Figure 21. Haralick's GLCM indices computed on the residual surface and DEM hillshade of a particular of the Caldera Blanca (Figure 14, spot 2).

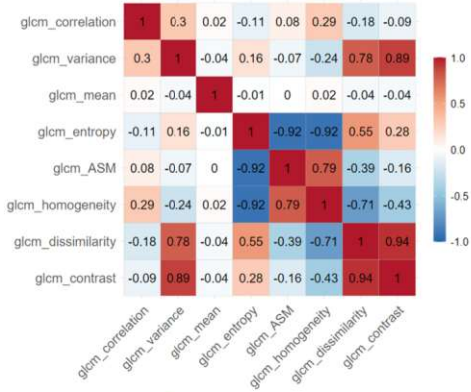

Figure 22. Correlation between Haralick's GLCM parameters. The strongly correlated parameters are (1) contrast, dissimilarity, and variance; (2) homogeneity, entropy, and ASM. In addition, the "glcm_mean" is essentially a smoothing of the residual surface. For this area, the parameters providing different information are variance, entropy, and correlation.

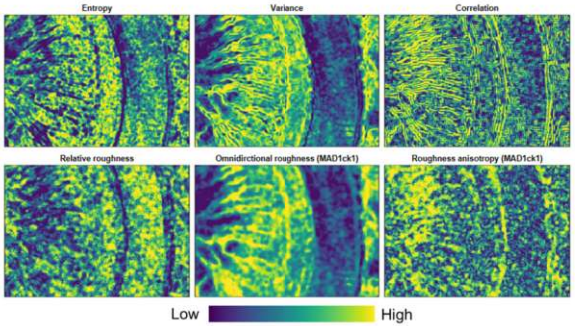

Figure 23. Selected GLCM parameters and three geostatistics-based indices (short-range omnidirectional roughness, short-range roughness anisotropy, and relative roughness) for a particular of the Caldera Blanca (Figure 14, spot 2). Color scale histogram equalized (quantile classification).

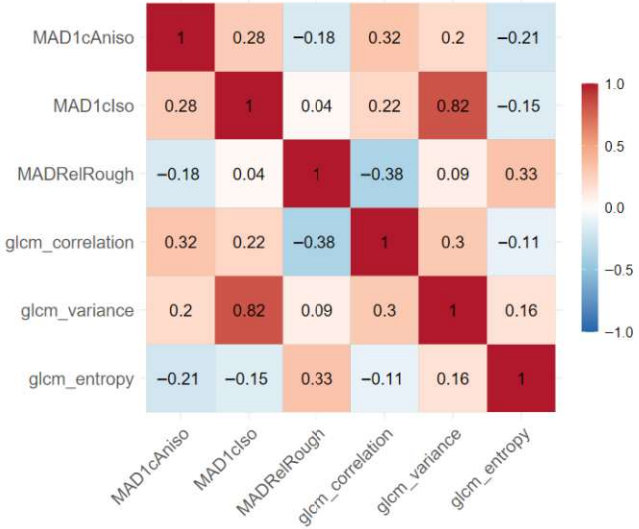

Figure 24. Correlation between selected GLCM indices and geostatistics-based indices. MAD1cAniso: short-range roughness anisotropy; MAD1cIso: short-range omnidirectional roughness; MADRelRough: relative roughness.

The binary or multiclass classification of elevation values, underlying the TT approach and GLCM, opens the way to more complex approaches such as LBP and geomorphons [117]. Other analogies can be found in geostatistics with the application of indicator coding [55]. Derivation of a drainage network and analysis of its spatial patterns, including drainage density, provide a related example of ST analysis (e.g., [172,173]). Once the pixels are classified in binary or multiclass values, the ST can be characterized by a wide range of methods, including the ones adopted in ecology providing different landscape patterns metrics, such as FRAGSTAT [174,175]. Accordingly, the analysis of transformed continuous surfaces into quantized pixels or segmented features (e.g., [21]) is another pathway for deriving more complex indices of ST. However, like other more complex methods, this approach provides high flexibility at the price of a high level of subjectivity in relation to the multiple calculation parameters and user decisions to be made. In addition, complex indices generally require more data with respect to simpler indices for their estimation, and hence larger search windows, which increase the likelihood of nonstationary conditions.

The SR indices can also be customized for specific purposes. The RRI provides an average of directional SR computed along eight directions with respect to the central pixel. The radial computation of SR is particularly interesting for ecology because it computes the

SR from the perspective of the central pixel, which could represent an animal that needs to move in the landscape [3,4]. However, it is likely that animals will select the smoothest direction, and will not really be interested in the average SR. Accordingly, in this setting the direction with minimum SR could be the feature one wants to catch. The possibility to customize ST indices is extremely wide (e.g., [169]), especially when moving toward multipoint statistics [60].

4.3. DDs of Higher Order and the Filtering of Curvature

RRI, geostatistical, and spectral methods have as a key ingredient DDs of various orders, which can ultimately be seen as directional filters. In addition, as reported above, the DDs of different orders have clear analogies with wavelets and the filters used in multiscale image analysis. DDs have the good characteristic of being easily interpretable in geomorphometric terms and at the same time providing effective directional filters for multiscale ST analysis. These kinds of directional filters can be manipulated and modified to derive multiscale ad hoc ST indices and can be extended to multipoint statistics.

A simple example of customization is represented by the possibility to derive SR indices that are unaffected by both the local slope and by local curvature [132]. The RRI and MAD_{k2} essentially exploit the capability of DDs of order 2 to filter out a first order trend, essentially the local slope. Figure 16 shows that both the RRI as well as omnidirectional roughness computed with MAD_{k2} tend to highlight, even if much less than the other conventional SR indices, some linear features that are locally smooth but with high curvatures such as the ridge of the craters, the change in slope at the foot slopes of the craters, and some lobate sediment deposit from flow processes inside the Caldera Blanca. This happens because order 2 DDs cannot filter a curved surface, such as a quadratic or a cubic surface; to do this it is necessary to use higher order differences, e.g., of order 3 and 4. Order 4 (Section 2.3) is particularly convenient. Using an odd number of elements, it allows for computation with respect to the central pixel, thereby eliminating the need for averaging processes. Filtering a third order polynomial, it can handle quite complex curved morphologies. In addition, the third is the lowest order polynomial that can be fitted in a 5×5 window for deriving changes in curvatures and for studying variability in curvature [127,128]. This can be particularly interesting for interpreting and analyzing SR in the context of physical-based geomorphometry [20]. Figure 25 presents the application of the conventional RRI, which uses second order DDs; the RRI with fourth order DDs; and MAD [111,125] with DDs of the second (MAD_{k2}) and fourth orders. Both for the RRI as well as for MAD, the main spatial patterns do not change with the different orders, except when corresponding to smooth curved surfaces, like the caldera ridges and the change in slope between the caldera flanks and the surrounding plain. Linear scarps, being non locally smooth, are preserved with DDs of the fourth order. It should be noted that the RRI with fourth order DDs is noisier than the conventional RRI; this increase in noise is not observed with MAD, due to the robustness of the median estimator.

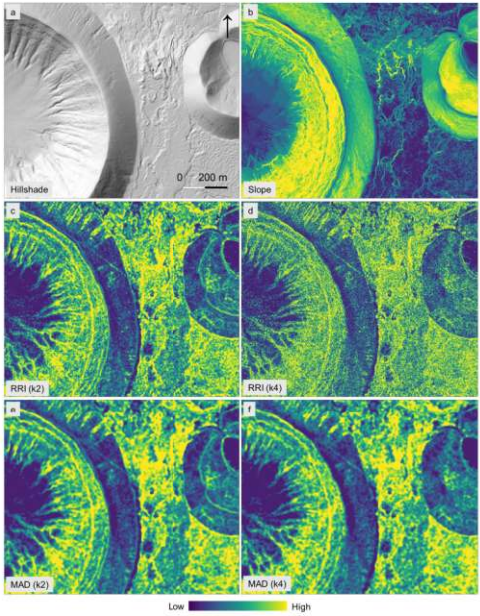

Figure 25. Filtering of local curvature using fourth order increments, for the RRI and omnidirectional short-range roughness based on MAD estimator. (**a**) Hillshade; (**b**) slope; (**c**) conventional RRI (second order increments); (**d**) RRI with fourth order increments; (**e**) MAD with second order increments; (**f**) MAD with fourth order increments. Color scales histogram equalized.

4.4. Multiscale Analysis

The possibility of computing the SR metrics at multiple scales amplifies their informative content and permits us to derive new SR indices. Depending on the objective of the analysis and the SR metrics adopted, the multiscale analysis can be conducted via different levels of smoothing, maintaining the same resolution or via multiresolution approaches (e.g., [32,94,167]). When using lag-dependent metrics, such as geostatistical ones, a multiresolution approach is particularly convenient, because decreasing the resolution increases the lag distance while maintaining the same kernel. There can be variations in the way in which the image is smoothed and/or upscaled, but the principle is to apply the chosen SR metrics, or any LSP, at multiple levels, analogous to wavelets approaches [65,92,118,119].

The multiscale SR indices can be manipulated to derive new indices, with a high diversity of extractable information. The new indices can be just simple statistical indices

(minimum, maximum, average, etc.) of the multiscale indices, or indices for specific scales of variation. Some authors (e.g., [22]) locate the scale at which a given SR index is maximum or at which scale (if any) the SR index begins to stabilize, in analogy to the variogram range and sill or to the "grain" of Pike [67]. The autocorrelation of the selected SR index across different scales may reveal interesting behaviors (e.g., [32]). Due to spatial continuity, bulk measures of SR tend to be correlated among scales, while other indices, such as SR anisotropy, can have quite sharp variations in correlation with scale [32]. In addition, spatial variability indices, such as geostatistical indices, can be applied directly for fractal analysis, to assess the presence of scale invariance and, in positive cases, estimate the fractal dimension [1,51,124].

The adoption of multiscale SR indices can provide effective tools for the expert-based interpretation of terrain patterns. It is possible to use RGB images (Figure 26), associating the SR indices calculated at different scales with the three bands (Figure 27). This representation can provide powerful tools for the expert-based visual interpretation of the landscape, for example, in the context of geomorphological and geological mapping. A full exploitation of multiscale SR indices can be achieved using these as input features for unsupervised and supervised machine learning approaches [25,30,32,35,113,176–179]. From this perspective there is some analogy to what is carried out internally with convolutional neural networks (e.g., [180]), with the difference that the convolutional filters are here defined by the user and are directly interpretable from a geomorphometric point of view.

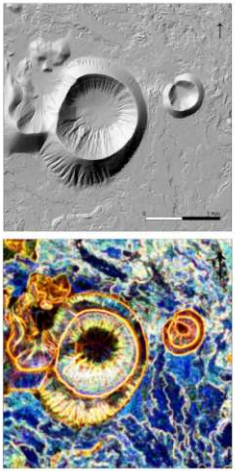

Figure 26. RGB image (each band is histogram equalized) using multiscale omnidirectional roughness indices, computed with MAD_{k2} (lag 1 pixel). Red level 4, Green level 2, and Blue level 1 (Figure 27). This combination of components of SR highlights the main morphological features of the landscape around Caldera Blanca, such as gold showing major breaks in slope.

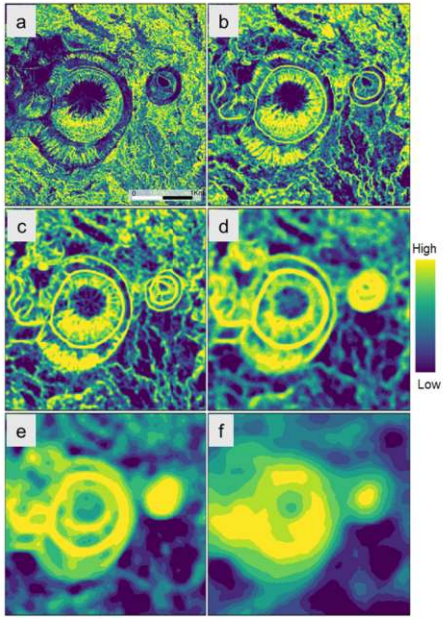

Figure 27. Omnidirectional MAD_{k2} for a lag of one pixel computed at different resolutions. The number of the level indicates the upscaling factor of the original DEM resolution (2 m). (**a**) Level 1; (**b**) level 2; (**c**) level 4; (**d**) level 8; (**e**) level 16; (**f**) level 32. The first two levels differentiate very well between lava flow deposits and the gullies along the Caldera Blanca's slopes. Level 4 highlights both gullies and lobate sedimentary deposits on the bottom of the caldera. The third, fourth, and fifth levels highlight quite well the transitions between lava flow deposits characterized by different fine-grain roughness. The last level (level 32) highlights the main volcanic structures without highlighting the ridges and the change in slope along the flanks of the calderas.

5. Discussion and Conclusions

In geomorphometry, SR, or more accurately, ST, should not be reduced to the mere computation of some morphometric derivatives. Instead, it should evolve into a self-consistent subfield, integrating insights from other geomorphometric approaches and serving as a key concept for extracting geomorphometric signatures. For instance, ST indices can complement physically based geomorphometry and support automated mapping techniques. The term SR should be used for indices computing some form of fine-grain variability in terms of pixels, hence generally referring to small windows and/or short lag distances.

However, this does not resolve ambiguities in terminology when performing the multiscale calculation of these indices. In addition, even when considering small windows and basic SR indices, there are different aspects of ST that can be extracted, making the selection of an index non-trivial. This selection should be based on both the purpose of the study and the characteristics of the data, including the terrain patterns. In the case of heterogeneous morphologies, especially when using high-resolution DEMs, we suggest considering SR indices based on robust estimators. From this perspective, a natural choice is to adopt flexible approaches such as MAD_{k2}, or to modify popular indices such as STDslope or STDres by replacing the standard deviation with a robust estimator of dispersion, such as the interquartile range, and using IQRslope and IQRres. For a pixel-centered (radial) analysis of SR, we strongly recommend the improved Radial Roughness Index (RRI) over the popular TRI.

When using small search windows (e.g., 5×5 pixels or a 3-pixel radius), the complexity of ST is constrained by the limited spatial domain. Even within these small windows, basic SR indices show significant differences, which become even more pronounced when analyzing specific textural aspects like SR anisotropy. As the window size increases or a multiscale analysis is performed, the variety and complexity of describable surfaces grow substantially. This leads to the need to use more complex ST indices for surface characterization. Therefore, a structured framework is essential to clarify the characteristics and limitations of the multitude of available indices and approaches. Such a framework also helps to theoretically interpret these indices and reveal analogies between seemingly different methods, as exemplified by the connection between geostatistical approaches and wavelets.

A relevant challenge toward a coherent framework of geomorphometric analysis of ST is the lack of consensus regarding terminology and definitions. It is crucial to distinguish between algorithmic interpretations from a geocomputational/mathematical perspective, and morphogenetic interpretations related to landform evolution. The same algorithm may emphasize different morphogenetic aspects depending on study area characteristics and scale of analysis (e.g., resolution). The RRI measures radial variability independently from the size of the pixel. However, according to the geomorphological perspective, the RRI can represent either roughness (short-range variations) or ruggedness (long-range variations), depending on the DEM resolution. Accordingly, the terminology and definition of an ST index should reflect the specific aspect of ST it highlights, independently from the absolute scale and the subsequent process-based interpretation. A circular pattern remains circular, independently from the absolute scale and the genetic process. It can be equally related to dolines or to volcanic craters. As another example, a set of highly anisotropic features can be related to a set of fractures in a rocky outcrop or to parallel gullies. Scale-dependent parameters, such as DEM resolution, search window geometry, and lag distances, must be explicitly defined when computing ST indices. This is fundamental for the interpretation of morphology according to morphogenetic processes and for the characterization and modeling of surface processes. Such an approach could foster synergies with related fields like surface metrology and image analysis, while preserving the interpretability of computed ST indices.

We think that developing new ST indices following a methodological framework like geostatistics can yield simple, interpretable, and robust metrics with minimal user-defined parameters and thus better comparability when applied in different studies. This approach can be extended to other flexible methods, such as spectral and fractal analyses, with the overarching goal of creating intuitive ST indices that capture key aspects of surface texture. Regardless of the method, multiscale analysis often remains essential.

Significant work remains on multiple fronts, likely requiring collaborative efforts beyond a single research group. A broad, participatory approach engaging researchers and end-users should be encouraged, fostering cross-disciplinary exchanges with fields like surface metrology, image analysis, and pattern recognition. Establishing consensus on terminology and definitions would be valuable, but one of the greatest challenges lies in creating an atlas of surface textures (AST), fundamental for creating real and synthetic benchmark datasets for testing, comparing, and validating ST algorithms. With these foundations, future research can focus on developing new indices for specific patterns and systematically categorizing existing ones. We provide, as documented in Appendix C, a set of tiles representing a sample of surface textures. Even if the sets provided represent an extremely small sample of possible surface textures, these highlight the potential and challenges behind the creation of an AST.

A key research question concerns the role and impact of artificial intelligence (AI) on ST analysis, particularly within predictive applications such as automatic mapping and landscape segmentation. A major challenge is whether the interpretability provided by well-defined ST indices will be lost to generative AI approaches that rely on a self-adaptive generation and tuning of input features. Hopefully, hybrid approaches will be capable of successfully merging the predictive power of self-adaptive models with the interpretability of geomorphometric science.

Author Contributions: Conceptualization, S.T. and P.L.G.; investigation S.T.; visualization, S.T.; writing—review and editing, S.T. and P.L.G. All authors have read and agreed to the published version of the manuscript.

Funding: This research received no external funding.

Data Availability Statement: The test high resolution DTM of the "Caldera Blanca" has been derived by means of interpolation of the point clouds downloaded from the website of the General Directorate of the National Geographic Institute of Spain and are covered by CC-BY 4.0 license [160]. Accordingly, the derived digital terrain model and the RGB imagery are a "Obra derivada de LiDAR-PNOA-cob3 2022-2025 CC-BY 4.0 scne.es" and are available in Zenodo [161]. The Copernicus DEM at 30 m (GLO 30 [181]) is available with open license at [145]. In [182], a set of selected surface texture tiles discussed in Appendix C is available.

Acknowledgments: Thanks to the International Society for Geomorphometry community (ISG, https://www.geomorphometry.org/) for the many exchanges of ideas.

Conflicts of Interest: The authors declare no conflicts of interest.

Abbreviations

The following abbreviations are used in this manuscript:

AOI	Area of interest
ASM	Angular second-moment (GLCM), measure of homogeneity of the image
AST	Atlas of surface textures
DD	Directional difference (e.g., for computing a variogram or MAD)
DEM	Digital elevation model
DOGs	Difference of Gaussians
DSM	Digital surface model
DTM	Digital terrain model
GLCM	Gray level cooccurrence matrix
IQRres	Interquartile range of residual surface (robust version of STDres)
IQRslope	Interquartile range of slope (robust version of STDslope)
LBP	Local binary pattern

LSP	Local surface parameter
MAD	Median absolute difference (applicable to DDs of any order)
NVD	Normal vector dispersion (also known as VRM)
RRI	Radial roughness index (improvement of TRI)
SA	Surface-area roughness index
SR	Surface roughness
ST	Surface texture
STDres	Standard deviation of residual surface
STDslope	Standard deviation of slope
TRI	Topographic ruggedness index
TT	Terrain texture
VRM	Vector ruggedness measure (analogous to NVD)

Appendix A. Theoretical Hints

Appendix A.1. Multiscalarity According to Dispersion Variance

The principle of multiscale analysis can be introduced intuitively, referring to moving averages and the concept of dispersion variance [102], well known in remote sensing and geostatistics [90]. Indeed, smoothing with moving averages, i.e., fitting a local polynomial of order 0 or performing a convolution with a square wave, means filtering out the variance inside the search window. Larger windows filter more spatial variability, leaving features with longer wavelengths in the smoothed DEM and with shorter wavelengths (fine-scale morphology) in the residual topography. The conventional formulation of the experimental variance does not consider the spatial support of measurements. For a given set of pixel values z_i sampled in some locations of a spatial domain (the AOI), the experimental variance [102] is as follows (Equation (A1)):

$$\sigma^2 = \frac{1}{n}\sum_{i=1}^{n}(z_i - m)^2 \quad \text{(A1)}$$

where m is the mean of the set of values z_i within the considered spatial domain.

However, with spatial data the spatial support, or 2D area, of measurements should be considered, given that it should not necessarily be punctual [114]. In addition, if the samples are aggregated in spatial subdomains covering the study area, the subdomain spatial support can be considered as well. Accordingly, in a spatial context, the formulation (Equation (A2)) of variance [102] considers the specific spatial support of the samples (s_a) and the spatial support of the (sub)domains/blocks within which variance is computed (s_b):

$$\sigma^2(s_a, s_b) = \frac{1}{n}\sum_{i=1}^{n}\left(z_{is_a} - m_{s_b}\right)^2 \quad \text{(A2)}$$

This formulation expresses the total variance in different components of spatial variability. A DEM or an image covering an AOI of size s_c and with pixels of size s_a, can be divided into blocks of size s_b (e.g., 3×3 pixels of size s_a). Accordingly, the total variance of pixels with support size s_a over the domain s_c can be decomposed in two components (Equation (A3)): the average variability of pixels inside the blocks of size s_b, and the variability of block values s_b within the whole domain (s_c):

$$\sigma^2(s_a, s_c) = \sigma^2(s_a, s_b) + \sigma^2(s_b, s_c) \quad \text{(A3)}$$

The approach can be nested to multiple scales, hence isolating specific components of spatial variability. The same is true, but more analytically complex and theoretically powerful, when adopting Gaussian smoothing [92,93], where the level of smoothing (and

the spatial scale) is controlled by the standard deviation. Ultimately it is a weighted average, with weights defined by a 2D Gaussian function.

Appendix A.2. Robustness of Geostatistical Estimators

Regarding geostatistical approaches (Figure A1), the impact of using nonrobust estimators can be observed by comparing the variogram, the madogram and the robust MAD [55,102,125]. The madogram and the variogram can be seen as members, respectively, with an exponent of 1 and 2 (Equation (A4)), of the general estimator based on (half) the mean of the N absolute DDs raised by a power p found in the search neighborhood. The DDs are represented by differences in the property of interest, e.g., residual surface or elevation, considering sample pairs separated by the vector h (the lag), i.e., $z(u)$ and $z(u + h)$. These equations consider DDs of the first order, but the same estimator can be extended to DDs of any order [55,110,111]. According to Equation (A4), the higher the exponent, the higher the sensitivity to outliers and nonstationarity. MAD, using the median estimator (Equation (A5)), is a much more robust estimator [55,125], and its robustness is independent from the exponent p.

$$\gamma(h)_p = \frac{1}{2N(h)} \sum_{\alpha=1}^{N(h)} |z(u_\alpha) - z(u_\alpha + h)|^p = \frac{1}{2} \cdot \text{mean}\left(|\Delta(h)|^p\right) \quad \text{(A4)}$$

With $\Delta(h_\alpha) = z(u_\alpha) - z(u_\alpha + h)$ and $\Delta(h)$ the set of all $\Delta(h_\alpha)$

$$\text{MAD}(h) = |\Delta(h)_{\alpha=median}| \quad \text{(A5)}$$

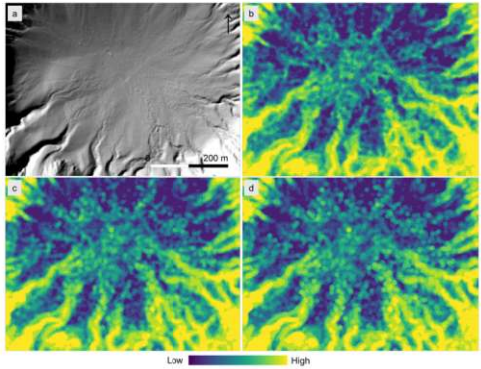

Figure A1. Estimation of omnidirectional roughness for a lag of one pixel with DDs of order 2, with different geostatistical estimators with decreasing levels of robustness to outliers and nonstationarity. (**a**) Hillshade; (**b**) MAD (m); (**c**) madogram (m); (**d**) variogram (m^2). The less robust the estimator, the more blurred and spottier the SR will appear. The choice to use MAD instead of madogram may depend on several factors: level of smoothing of the DEM, characteristics of morphology, and presence of artifacts.

Appendix B. Complex Terrains Examples

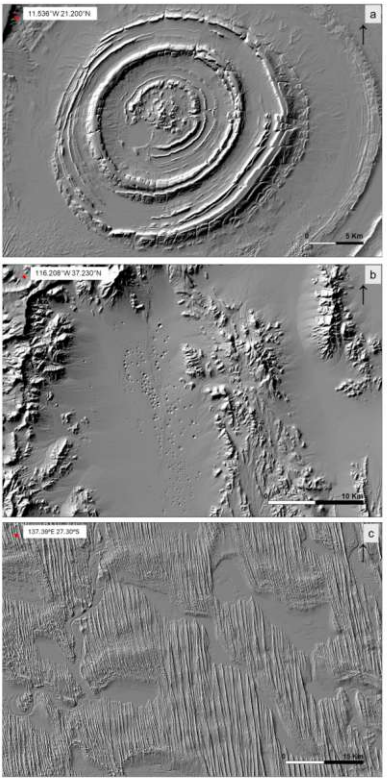

Figure A2. *Cont.*

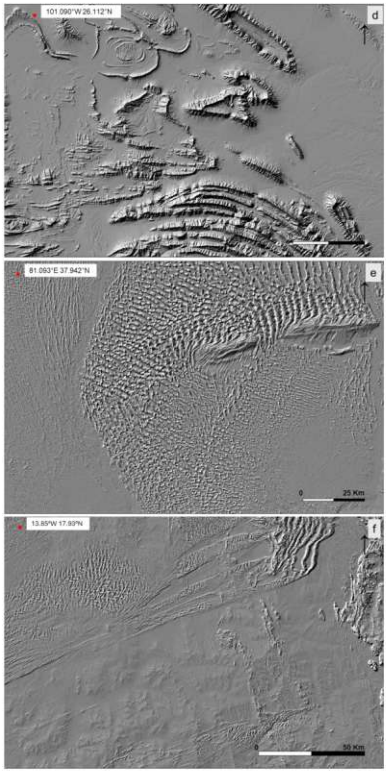

Figure A2. Hillshades from Copernicus DEM (UTM re-projected, 30 m resolution), arranged from smallest to largest areas, covering different environments and extents, highlighting the complexity of real terrains. (**a**) Eye of the Sahara, Mauritania; (**b**) "nuclear karst", Nevada, USA; (**c**) Simpson desert, Australia; (**d**) Monterrey, Nuevo León, state, Mexico; (**e**) Taklimakan desert, China; (**f**) Mauritania desert.

Appendix C. The Challenges for an Atlas of Surface Textures

The design and implementation of an atlas of surface textures (AST), intended to be a multipurpose collection of textures, present many challenges and constraints. A key use

of the AST is the creation of benchmark data for testing and comparing ST indices and algorithms. The following discussion focuses on an initial implementation using raster DEMs on land.

A prototype AST can be built from existing open-license data, such as high-resolution digital terrain and surface models (DTMs/DSMs) derived from lidar. Many national and regional agencies provide such HR-DEMs. These datasets are typically offered as 1–2 m rasters, accompanied by metadata on the survey parameters (sensor, flight elevation, point density) and quality estimates, often including vertical error standard deviation (commonly around 0.25 m) derived from ground control points.

High point density in the underlying lidar point clouds and low reported error do not guarantee a high-quality product. Potential data tiles must undergo quality checks before inclusion in the AST. A critical first step is a visual assessment using various geomorphometric derivatives to identify artifacts and evaluate the representation of surface morphology. This visual analysis should extend beyond hillshade, at a minimum, generating a residual surface, a simple yet effective sharpening technique that highlights artifacts and fine-scale features.

The prototype AST contains 64 tiles in northern Italy and is structured as a GIS database. This allows for the plotting of the tile locations on a base map and the filtering of the database to restrict the records displayed and used. Table A1 shows the structure of a record from the database, and Figure A3 shows hillshade maps for the tiles with river or stream features. The prototype allows us to experiment with the structure and design decisions, to improve the database, and expand to other areas and features. The prototype is currently posted on GitHub (https://github.com/strevisani/atlas-of-surface-textures, accessed on 25 November 2025) and is a work in progress. We encourage collaborative contributions.

Table A1. Database structure.

FIELD NAME	SAMPLE FIELD CONTENTS
ID	8
DEM_NAME	friuli_riverbed1.tif
FEATURES	active riverbed
COMPLEX	NO
PIXEL_M	2
PIXELS	256
LAT	46.2507447
LONG	13.0450478
SURVEY	Rilievo LIDAR RAFVG 2017–2020
SOURCE	https://irdat.regione.fvg.it/consultatore-dati-ambientali-territoriali/detail/irdat/dataset/11826, accessed on 25 November 2025
LICENSE	ITALIA OPEN DATA LICENSE V2.0 (IODL 2.0)

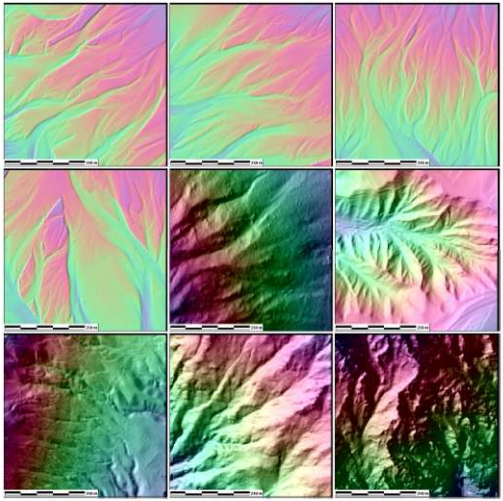

Figure A3. Riverbeds and channels from the AST protype.

Eventual extensions to the AST include the following, which we expect to be a natural follow-on as we work with the prototype:

- More complex and larger tiles;
- Extension to other DEM resolutions, such as the global 1-arc-second DEMs;
- Bathymetry and planetary DEMs;
- Lidar point clouds in addition to DEMs;
- Adding fields like "Setting", "Morphology", or "Type of pattern".

Challenges we see in extending the AST:

- Algorithmically defining complex tiles, examples of which are included in Appendix B, instead of picking visually.
- Handling complex tiles with different textural domains. Should we mask out to leave only a single feature in the tile, or index the tile to separate the different features with either a vector or raster mask file?
- Differentiating features/objects/landforms from textures.
- Handling coalescent spatial textures and texture transitions.

Our AST has some similarities with the work of Kennelly and others [183,184]. They started at larger scale, with 10 DEMs demonstrating complex archetypal landforms. A key aim of the AST, however, is to provide an extensive collection of surfaces from which subsets of texture tiles can be easily extracted. The AST tiles are intended for designing, testing, and benchmarking surface texture algorithms. The work of Kennelly and others

also highlights the challenges in building a larger database and influenced our decision to start with smaller tiles and generally simpler and less complex areas. Another source of inspiration is represented by the USGS set of one hundred paper topographic maps illustrating specified physiographic features, which surprisingly has a very limited online presence (https://catalogue.nla.gov.au/catalog/6889264, accessed on 25 November 2025). A digital equivalent of this USGS set would be highly desirable.

Appendix D. Basic Roughness Algorithms and Implementing Software

Table A2. Basic surface roughness algorithms and software discussed in Section 4.1.3. For complex algorithms, the references are reported with a detailed description.

Acronym	Algorithm Description	Software
MAD_{k2} [111,125]	• Compute absolute second order DDs (0.5, 1, or 2 pixels lag) along four directions (cardinal and diagonal) • Compute MAD_{k2} in the four directions for a given search window • Derive omnidirectional SR and SR anisotropy	ArcGIS Pro 3.6 (toolbox MADk2) MICRODEM Nov 2025 (GUI, command line, source code) SurfRough v1.1 R package (Madscan)
RRI [131]	• Average of absolute DDs computed radially with respect to the focal pixel	ArcGIS PRO 3.6 (toolbox ArcRRI) MICRODEM Nov 2025 (GUI, command line, source code) QGIS 3.4 (processing toolbox RRI) SurfRough v1.1 R package (function RRI)
NVD [13]	• Compute slope and aspect • Derive normal vector components • Compute circular dispersion (resultant length approach)	ArcGis Pro 3.6, Topography Toolbox (VRM) GRASS 8 (r.vector.ruggedness) MultiscaleDTM v1.0 R package (VRM) SAGA 9 (Vector Ruggedness Measure, VRM) SurfRough v1.1 R package (circularDispersionNV) Whitebox v2.4 (SphericalStdDevOfNormals, normalized version of NVD)
STDslope	• Compute slope • Compute standard deviation in the search window	GISs permitting focal statistics/functions MICRODEM Nov 2025 (GUI, command line, source code) Terra v1.8-80 R package (slope computation and focal function)
STDres	• Compute residual elevation • Compute standard deviation in the search window	GISs permitting focal statistics/functions MICRODEM Nov 2025 (GUI, command line, source code) MultiscaleDTM v1.0 R package (AdjSD, RIE) Terra v1.8-80 R package (map algebra and focal functions)
IQRslope [introduced here]	• Compute slope • Compute IQR in the search window	GISs permitting focal statistics/functions MICRODEM Nov 2025 (GUI, command line, source code) Terra v1.8-80 R package (slope computation and focal function)
IQRres [introduced here]	• Compute residual elevation • Compute IQR in the search window	GISs permitting focal statistics/functions MICRODEM Nov 2025 (GUI, command line, source code) Terra v1.8-80 R package (map algebra and focal functions)
SA [50,108]	Compute pixel area in 2D and 3D (correcting for slope) using elevations, and then find ratio of two areas	MultiscaleDTM v1.0 R package (SAPA)

Table A3. Websites for programs/code computing roughness reported in Table A2.

Program/Code	Program Websites
ArcGISPro	https://www.esri.com/en-us/arcgis/products/arcgis-pro/overview, accessed on 25 November 2025 toolbox ArcRRI e MADk2: https://github.com/strevisani/MADSurfaceTexture/tree/master/ArcGisProScripts, accessed on 25 November 2025
GRASS	https://grass.osgeo.org/learn/manuals/, accessed on 25 November 2025
MICRODEM	https://github.com/prof-pguth/git_microdem, accessed on 25 November 2025 https://microdem.org/, accessed on 25 November 2025
MultiscaleDTM	https://cran.r-project.org/package=MultiscaleDTM, accessed on 25 November 2025 https://github.com/ailich/MultiscaleDTM, accessed on 25 November 2025 https://zenodo.org/records/15476682, accessed on 25 November 2025
QGIS	https://qgis.org/, accessed on 25 November 2025 RRI toolbox: https://github.com/strevisani/MADSurfaceTexture/tree/master/Qgis, accessed on 25 November 2025
SAGA	https://sourceforge.net/projects/saga-gis/, accessed on 25 November 2025
SurfRough	https://cran.r-project.org/package=SurfRough, accessed on 25 November 2025 https://doi.org/10.5281/zenodo.7132160, accessed on 25 November 2025 https://github.com/strevisani/SurfRough, accessed on 25 November 2025
Whitebox	https://www.whiteboxgeo.com/download-whiteboxtools/, accessed on 25 November 2025

Appendix E. Glossary of Key Terms

Definition and intended interpretations of key terms used in this paper.

Complexity (topographic)	The term complexity is used in the text in a conventional and non-mathematical meaning. We do not propose a quantitative definition. A complex topography cannot be described quantitatively by a simple model with few parameters and is difficult to understand or conceptualize. It typically involves nonstationary spatial structures, multiple overlapping patterns, and interruptions in spatial continuity.
Dispersion variance	The (spatial) variance of a variable that arises specifically from the geometry (extent and shape) of the spatial support of measurement. Tendentially, at least in presence of spatial correlation, as the support size increases the variance decreases.
Form/structure	In surface metrology, a fundamental distinction is made between "form" (the general, intended shape of an object) and "texture" (local deviations from that shape). This concept is scale-dependent and presents ambiguities. The concept of "form" is analogous to the "trend" in geostatistics and to "landform" in geomorphometry. A set of contiguous landforms can itself constitute a texture at a broader scale.
Hotspot	A localized area (e.g., a single pixel) where the value of a measured variable (e.g., elevation, residual surface, slope, etc.) is significantly higher/lower than the background or surrounding area.
Local binary pattern	A texture descriptor that encodes the local pattern around a pixel by comparing it to its neighbors, considering a specific search radius.
Spatial continuity	The empirical observation that values at nearby geographic locations are, on average, more similar than values at locations farther apart. Tools like the covariance, autocorrelation, variogram, and madogram are bivariate functions used to model this spatial dependence.

Spatial support	The size, geometry, and orientation of the area/volume on which data is measured (e.g., a topographic ground control point) or to which estimates are made (e.g., a large pixel size). Changing the support dramatically affects the measured value and its variance.
Spatial variability structure	From a geostatistical perspective, it refers to the statistical spatial law governing a spatial phenomenon, which is conceptualized as a realization of a Random Function. The variogram and covariance functions are key statistical moments used to describe some features of this spatial law.
Stationarity	Assumption/requirement that the key statistical properties (e.g., the mean and the spatial covariance) of a spatial process are uniform throughout the region of interest.
Wavelets	A set of mathematical functions used for multi-resolution analysis. These can be used for filtering, denoising spatial data, or characterizing complex, multi-scale spatial patterns.

References

1. Shepard, M.K.; Campbell, B.A.; Bulmer, M.H.; Farr, T.G.; Gaddis, L.R.; Plaut, J.J. The Roughness of Natural Terrain: A Planetary and Remote Sensing Perspective. *J. Geophys. Res. Planets* **2001**, *106*, 32777–32795. [CrossRef]
2. Smith, M.W. Roughness in the Earth Sciences. *Earth-Sci. Rev.* **2014**, *136*, 202–225. [CrossRef]
3. Riley, S.J.; DeGloria, S.D.; Elliot, R. A Terrain Ruggedness Index That Quantifies Topographic Heterogeneity. *Intermt. J. Sci.* **1999**, *5*, 23–27.
4. Sappington, J.M.; Longshore, K.M.; Thompson, D.B. Quantifying Landscape Ruggedness for Animal Habitat Analysis: A Case Study Using Bighorn Sheep in the Mojave Desert. *J. Wildl. Manag.* **2007**, *71*, 1419–1426. [CrossRef]
5. Blair, T.C.; McPherson, J.G. Grain-Size and Textural Classification of Coarse Sedimentary Particles. *J. Sediment. Res.* **1999**, *69*, 6–19. [CrossRef]
6. Cavalli, M.; Marchi, L. Characterisation of the Surface Morphology of an Alpine Alluvial Fan Using Airborne LiDAR. *Nat. Hazards Earth Syst. Sci.* **2008**, *8*, 323–333. [CrossRef]
7. Frankel, K.L.; Dolan, J.F. Characterizing Arid Region Alluvial Fan Surface Roughness with Airborne Laser Swath Mapping Digital Topographic Data. *J. Geophys. Res. Earth Surf.* **2007**, *112*, F02025. [CrossRef]
8. Mark, D.M. Geomorphometric Parameters: A Review and Evaluation. *Geogr. Annaler. Ser. A Phys. Geogr.* **1975**, *57*, 165–177. [CrossRef]
9. Pike, R.J. The Geometric Signature: Quantifying Landslide-Terrain Types from Digital Elevation Models. *Math. Geol.* **1988**, *20*, 491–511. [CrossRef]
10. Pike, R.J. Geomorphometry—Diversity in Quantitative Surface Analysis. *Prog. Phys. Geogr.* **2000**, *24*, 1–20. [CrossRef]
11. Olaya, V. Scale. *Dev. Soil Sci.* **2009**, *33*, 141–169. [CrossRef]
12. Fox, C.G.; Hayes, D.E. Quantitative Methods for Analyzing the Roughness of the Seafloor. *Rev. Geophys.* **1985**, *23*, 1–48. [CrossRef]
13. McKean, J.; Roering, J. Objective Landslide Detection and Surface Morphology Mapping Using High-Resolution Airborne Laser Altimetry. *Geomorphology* **2004**, *57*, 331–351. [CrossRef]
14. Glenn, N.F.; Streutker, D.R.; Chadwick, D.J.; Thackray, G.D.; Dorsch, S.J. Analysis of LiDAR-Derived Topographic Information for Characterizing and Differentiating Landslide Morphology and Activity. *Geomorphology* **2006**, *73*, 131–148. [CrossRef]
15. Grohmann, C.H.; Smith, M.J.; Riccomini, C. Multiscale Analysis of Topographic Surface Roughness in the Midland Valley, Scotland. *IEEE Trans. Geosci. Remote Sens.* **2011**, *49*, 1200–1213. [CrossRef]
16. Kreslavsky, M.A.; Head, J.W.; Neumann, G.A.; Rosenburg, M.A.; Aharonson, O.; Smith, D.E.; Zuber, M.T. Lunar Topographic Roughness Maps from Lunar Orbiter Laser Altimeter (LOLA) Data: Scale Dependence and Correlation with Geologic Features and Units. *Icarus* **2013**, *226*, 52–66. [CrossRef]
17. Vincent, J.-B.; Asphaug, E.; Barnouin, O.; Beccarelli, J.; Benavidez, P.G.; Campo-Bagatin, A.; Chabot, N.L.; Ernst, C.M.; Hasselmann, P.H.; Hirabayashi, M.; et al. Macroscale Roughness Reveals the Complex History of Asteroids Didymos and Dimorphos. *Planet. Sci. J.* **2024**, *5*, 236. [CrossRef]
18. Bertuzzi, P.; Rauws, G.; Courault, D. Testing Roughness Indices to Estimate Soil Surface Roughness Changes Due to Simulated Rainfall. *Soil Tillage Res.* **1990**, *17*, 87–99. [CrossRef]
19. Evans, B.R.; Möller, I.; Spencer, T.; Smith, G. Dynamics of Salt Marsh Margins Are Related to Their Three-Dimensional Functional Form. *Earth Surf. Process. Landf.* **2019**, *44*, 1816–1827. [CrossRef]
20. Minár, J.; Drăguţ, L.; Evans, I.S.; Feciskanin, R.; Gallay, M.; Jenčo, M.; Popov, A. Physical Geomorphometry for Elementary Land Surface Segmentation and Digital Geomorphological Mapping. *Earth-Sci. Rev.* **2024**, *248*, 104631. [CrossRef]

21. Jiao, H.; Cheng, J.; Li, F.; Ma, J.; Xu, X.; Yang, X.; Tang, G.; Wei, H. Quantifying Regional Differentiation of Yardang Groups Using Terrain Texture Indices. *Int. J. Digit. Earth* **2025**, *18*, 2539486. [CrossRef]
22. Lindsay, J.B.; Newman, D.R.; Francioni, A. Scale-Optimized Surface Roughness for Topographic Analysis. *Geosciences* **2019**, *9*, 322. [CrossRef]
23. Kaiser, A.; Neugirg, F.; Haas, F.; Schmidt, J.; Becht, M.; Schindewolf, M. Determination of Hydrological Roughness by Means of Close Range Remote Sensing. *SOIL* **2015**, *1*, 613–620. [CrossRef]
24. Williams, L.L.; Lück-Vogel, M. Comparative Assessment of the GIS Based Bathtub Model and an Enhanced Bathtub Model for Coastal Inundation. *J. Coast. Conserv.* **2020**, *24*, 23. [CrossRef]
25. Huang, G.; Yang, L.; Cai, Y.; Zhang, D. Terrain Classification-Based Rover Traverse Planner with Kinematic Constraints for Mars Exploration. *Planet. Space Sci.* **2021**, *209*, 105371. [CrossRef]
26. Ferguson, R.I.; Hardy, R.J.; Hodge, R.A.; Houseago, R.C.; Yager, E.M.; Yamasaki, T.N. Predicting Flow Resistance in Rough-Bed Rivers from Topographic Roughness: Review and Open Questions. *Earth Surf. Process. Landf.* **2024**, *49*, 4888–4907. [CrossRef]
27. Houseago, R.C.; Hodge, R.A.; Asher, B.; Ferguson, R.I.; Hackney, C.R.; Hardy, R.J.; Hoey, T.B.; Johnson, J.P.L.; Rice, S.P.; Yager, E.M.; et al. Quantifying Bed Surface Roughness in Bedrock and Boulder-Bed Rivers. *J. Geophys. Res. Earth Surf.* **2025**, *130*, e2024JF007996. [CrossRef]
28. Iwahashi, J.; Pike, R.J. Automated Classifications of Topography from DEMs by an Unsupervised Nested-Means Algorithm and a Three-Part Geometric Signature. *Geomorphology* **2007**, *86*, 409–440. [CrossRef]
29. Iwahashi, J.; Kamiya, I.; Matsuoka, M.; Yamazaki, D. Global Terrain Classification Using 280 m DEMs: Segmentation, Clustering, and Reclassification. *Prog. Earth Planet. Sci.* **2018**, *5*, 1. [CrossRef]
30. Trevisani, S.; Cavalli, M.; Marchi, L. Surface Texture Analysis of a High-Resolution DTM: Interpreting an Alpine Basin. *Geomorphology* **2012**, *161–162*, 26–39. [CrossRef]
31. Wang, Z.; Brenning, A. Unsupervised Active–Transfer Learning for Automated Landslide Mapping. *Comput. Geosci.* **2023**, *181*, 105457. [CrossRef]
32. Trevisani, S.; Guth, P.L. Terrain Analysis According to Multiscale Surface Roughness in the Taklimakan Desert. *Land* **2024**, *13*, 1843. [CrossRef]
33. Lucieer, A.; Stein, A. Texture-Based Landform Segmentation of LiDAR Imagery. *Int. J. Appl. Earth Obs. Geoinf.* **2005**, *6*, 261–270. [CrossRef]
34. Van Den Eeckhaut, M.; Kerle, N.; Poesen, J.; Hervás, J. Object-Oriented Identification of Forested Landslides with Derivatives of Single Pulse LiDAR Data. *Geomorphology* **2012**, *173–174*, 30–42. [CrossRef]
35. González-Díez, A.; Barreda-Argüeso, J.A.; Rodríguez-Rodríguez, L.; Fernández-Lozano, J. The Use of Filters Based on the Fast Fourier Transform Applied to DEMs for the Objective Mapping of Karstic Features. *Geomorphology* **2021**, *385*, 107724. [CrossRef]
36. Cetinkaya, S.; Kocaman, S. Snow Avalanche Susceptibility Mapping for Davos, Switzerland. In Proceedings of the International Archives of the Photogrammetry, Remote Sensing and Spatial Information Sciences—ISPRS Archives, Nice, France, 6–11 June 2022; Volume 43, pp. 1083–1090.
37. Su, C.; Wang, B.; Lv, Y.; Zhang, M.; Peng, D.; Bate, B.; Zhang, S. Improved Landslide Susceptibility Mapping Using Unsupervised and Supervised Collaborative Machine Learning Models. *Georisk* **2023**, *17*, 387–405. [CrossRef]
38. Bjånes, A.; De La Fuente, R.; Mena, P. A Deep Learning Ensemble Model for Wildfire Susceptibility Mapping. *Ecol. Inform.* **2021**, *65*, 101397. [CrossRef]
39. Wilson, M.F.J.; O'Connell, B.; Brown, C.; Guinan, J.C.; Grehan, A.J. Multiscale Terrain Analysis of Multibeam Bathymetry Data for Habitat Mapping on the Continental Slope. *Mar. Geod.* **2007**, *30*, 3–35. [CrossRef]
40. Dunn, D.; Halpin, P. Rugosity-Based Regional Modeling of Hard-Bottom Habitat. *Mar Ecol Prog Ser* **2009**, *377*, 1–11. [CrossRef]
41. Kaskela, A.M.; Kotilainen, A.T. Seabed Geodiversity in a Glaciated Shelf Area, the Baltic Sea. *Geomorphology* **2017**, *295*, 419–435. [CrossRef]
42. Lecours, V.; Oxton, A.; Khor, D.; Tiplea, J. High-Resolution Ensemble Modelling of Coral Distributions in the Northern Gulf of Mexico Based on Geomorphometry: Coral Diversity and Benthic Habitat Fragmentation From Oil and Gas Infrastructure to Inform Spatial Planning. *Aquat. Conserv. Mar. Freshw. Ecosyst.* **2024**, *34*, e4234. [CrossRef]
43. Liu, Y.-S.; Yigitcanlar, T.; Guaralda, M.; Degirmenci, K.; Liu, A. Spatial Modelling of Urban Wind Characteristics: Review of Contributions to Sustainable Urban Development. *Buildings* **2024**, *14*, 737. [CrossRef]
44. Nayyar, Z.A.; Ali, A. Roughness Classification Utilizing Remote Sensing Techniques for Wind Resource Assessment. *Renew. Energy* **2020**, *149*, 66–79. [CrossRef]
45. Kim, J.; Shin, H.-J.; Lee, K.; Hong, J. Enhancement of ANN-Based Wind Power Forecasting by Modification of Surface Roughness Parameterization over Complex Terrain. *J. Environ. Manag.* **2024**, *362*, 121246. [CrossRef] [PubMed]
46. Dachauer, A.; Hann, R.; Hodson, A.J. Aerodynamic Roughness Length of Crevassed Tidewater Glaciers from UAV Mapping. *Cryosphere* **2021**, *15*, 5513–5528. [CrossRef]

47. Brožová, N.; Baggio, T.; D'agostino, V.; Bühler, Y.; Bebi, P. Multiscale Analysis of Surface Roughness for the Improvement of Natural Hazard Modelling. *Nat. Hazards Earth Syst. Sci.* **2021**, *21*, 3539–3562. [CrossRef]
48. Hobson, R.D. *Surface Roughness in Topography: Quantitative Approach*; Chorley, R.J., Ed.; Methuen & CO Ltd.: London, UK, 1972; Volume 6.
49. Hobson, R.D. Surface Roughness in Topography: Quantitative Approach. In *Spatial Analysis in Geomorphology*; Routledge: Oxfordshire, UK, 2019; Volume 6.
50. Du Preez, C. A New Arc–Chord Ratio (ACR) Rugosity Index for Quantifying Three-Dimensional Landscape Structural Complexity. *Landsc. Ecol.* **2015**, *30*, 181–192. [CrossRef]
51. Bruno, R.; Raspa, G. Geostatistical Characterization of Fractal Models of Surfaces. In Proceedings of the Geostatistics; Armstrong, M., Ed.; Springer: Dordrecht, The Netherlands, 1989; pp. 77–89.
52. Xu, T.; Moore, I.D.; Gallant, J.C. Fractals, Fractal Dimensions and Landscapes—A Review. *Geomorphology* **1993**, *8*, 245–262. [CrossRef]
53. Bez, N.; Bertrand, S. The Duality of Fractals: Roughness and Self-Similarity. *Theor. Ecol.* **2011**, *4*, 371–383. [CrossRef]
54. Pardo-Igúzquiza, E.; Dowd, P.A.; Ruiz-Constán, A.; Martos-Rosillo, S.; Luque-Espinar, J.A.; Rodríguez-Galiano, V.; Pedrera, A. Epikarst Mapping by Remote Sensing. *Catena* **2018**, *165*, 1–11. [CrossRef]
55. Chilès, J.-P.; Delfiner, P. *Geostatistics: Modeling Spatial Uncertainty*, 2nd ed.; John Wiley & Sons: Hoboken, NJ, USA, 2012.
56. Herzfeld, U.C.; Higginson, C.A. Automated Geostatistical Seafloor Classification—Principles, Parameters, Feature Vectors, and Discrimination Criteria. *Comput. Geosci.* **1996**, *22*, 35–41. [CrossRef]
57. Hristopulos, D.T. *Random Fields for Spatial Data Modeling: A Primer for Scientists and Engineers*, 1st ed.; Advances in Geographic Information Science; Springer: Dordrecht, The Netherlands, 2020.
58. Herzfeld, U.C. Master of the Obscure—Automated Geostatistical Classification in Presence of Complex Geophysical Processes. *Math. Geosci.* **2008**, *40*, 587–618. [CrossRef]
59. Trevisani, S.; Cavalli, M.; Marchi, L. Variogram Maps from LiDAR Data as Fingerprints of Surface Morphology on Scree Slopes. *Nat. Hazards Earth Syst. Sci.* **2009**, *9*, 129–133. [CrossRef]
60. Mariethoz, G.; Lefebvre, S. Bridges between Multiple-Point Geostatistics and Texture Synthesis: Review and Guidelines for Future Research. *Comput. Geosci.* **2014**, *66*, 66–80. [CrossRef]
61. Stromberg, W.D.; Farr, T.G. A Fourier-Based Textural Feature Extraction Procedure. *IEEE Trans. Geosci. Remote Sens.* **1986**, *GE-24*, 722–731. [CrossRef]
62. Davis, J.D.; Chojnacki, J.D. Two-Dimensional Discrete Fourier Transform Analysis of Karst and Coral Reef Morphologies. *Trans. GIS* **2017**, *21*, 521–545. [CrossRef]
63. Booth, A.M.; Roering, J.J.; Perron, J.T. Automated Landslide Mapping Using Spectral Analysis and High-Resolution Topographic Data: Puget Sound Lowlands, Washington, and Portland Hills, Oregon. *Geomorphology* **2009**, *109*, 132–147. [CrossRef]
64. Wu, J.; Yang, Q.; Li, Y. Partitioning of Terrain Features Based on Roughness. *Remote Sens.* **2018**, *10*, 1985. [CrossRef]
65. Xu, Y.; Zhang, S.; Li, J.; Liu, H.; Zhu, H. Extracting Terrain Texture Features for Landform Classification Using Wavelet Decomposition. *ISPRS Int. J. Geo-Inf.* **2021**, *10*, 658. [CrossRef]
66. Guth, P.L. Quantifying Terrain Fabric in Digital Elevation Models. *GSA Rev. Eng. Geol.* **2001**, *14*, 13–25. [CrossRef]
67. Pike, R.J.; Acevedo, W.; Card, D.H. Topographic Grain Automated from Digital Elevation Models. In Auto-Carto 9. Proceedings of the International Symposium on Computer-Assisted Cartography, Baltimore, MD, USA, 2–7 April 1989; American Congress on Surveying and Mapping: Frederick, MD, USA, 1989.
68. Zawada, D.G.; Piniak, G.A.; Hearn, C.J. Topographic Complexity and Roughness of a Tropical Benthic Seascape. *Geophys. Res. Lett.* **2010**, *37*, L14604. [CrossRef]
69. MacMillan, R.A.; Jones, R.K.; McNabb, D.H. Defining a Hierarchy of Spatial Entities for Environmental Analysis and Modeling Using Digital Elevation Models (DEMs). *Comput. Environ. Urban Syst.* **2004**, *28*, 175–200. [CrossRef]
70. Keylock, C.J.; Singh, A.; Passalacqua, P.; Foufoula-Georgiou, E. Evaluating Landscape Complexity and the Contribution of Non-Locality to Geomorphometry. *J. Geophys. Res. Earth Surf.* **2021**, *126*, e2020JF005765. [CrossRef]
71. Sous, D.; Meulé, S.; Dealbera, S.; Michaud, H.; Gassier, G.; Pezerat, M.; Bouchette, F. Quantifying the Topographical Structure of Rocky and Coral Seabeds. *PLoS ONE* **2024**, *19*, e0303422. [CrossRef] [PubMed]
72. Whipple, K.X. Landscape Texture Set to Scale. *Nature* **2009**, *460*, 468–469. [CrossRef]
73. Perron, J.T.; Kirchner, J.W.; Dietrich, W.E. Formation of Evenly Spaced Ridges and Valleys. *Nature* **2009**, *460*, 502–505. [CrossRef]
74. Zomer, J.Y.; Vermeulen, B.; Hoitink, A.J.F. Coexistence of Two Dune Scales in a Lowland River. *Earth Surf. Dyn.* **2023**, *11*, 1283–1298. [CrossRef]
75. Leach, R. *Characterisation of Areal Surface Texture*, 2nd ed.; Springer: Cham, Switzerland, 2013; Volume 9783642364587.
76. Pike, R.J. Digital Terrain Modeling and Industrial Surface Metrology: Converging Realms. *Prof. Geogr.* **2001**, *53*, 263–274. [CrossRef]

77. Beyerer, J.; León, F.P.; Frese, C. *Machine Vision: Automated Visual Inspection: Theory, Practice and Applications*; Springer: Berlin/Heidelberg, Germany, 2015.
78. Evans, I.S. Geomorphometry and Landform Mapping: What Is a Landform? *Geomorphology* **2012**, *137*, 94–106. [CrossRef]
79. Minár, J.; Evans, I.S. Elementary Forms for Land Surface Segmentation: The Theoretical Basis of Terrain Analysis and Geomorphological Mapping. *Geomorphology* **2008**, *95*, 236–259. [CrossRef]
80. MacMillan, R.A.; Shary, P.A. Landforms and Landform Elements in Geomorphometry. *Dev. Soil Sci.* **2009**, *33*, 227–254.
81. Marr, D.; Hildreth, E.; Brenner, S. Theory of Edge Detection. *Proc. R. Soc. London. Ser. B. Biol. Sci.* **1980**, *207*, 187–217. [CrossRef] [PubMed]
82. ASME. *Surface Texture (Surface Roughness, Waviness, and Lay)*; American Society of Mechanical Engineers: New York, NY, USA, 2019.
83. *ISO 25178-2:2021*; ISO Geometrical Product Specifications (GPS)—Surface Texture: Areal—Part 2: Terms, Definitions and Surface Texture Parameters. ISO: London, UK, 2021.
84. Taylor Hobson Limited. *Exploring Surface Texture A Fundamental Guide to the Measurement of Surface Finish*, 7th ed.; Taylor Hobson Limited: Leicester, UK, 2011.
85. R Core Team. *R: A Language and Environment for Statistical Computing*; R Foundation for Statistical Computing: Vienna, Austria, 2025.
86. Hijmans, R.J. *Terra: Spatial Data Analysis*; R Foundation for Statistical Computing: Vienna, Austria, 2025.
87. Trevisani, S. MADSurfaceTexture: V1.1 Plus R Package. 2023. Available online: https://doi.org/10.5281/zenodo.7132160 (accessed on 25 November 2025).
88. Pollyea, R.M.; Fairley, J.P. Estimating Surface Roughness of Terrestrial Laser Scan Data Using Orthogonal Distance Regression. *Geology* **2011**, *39*, 623–626. [CrossRef]
89. Fan, L.; Atkinson, P.M. A New Multi-Resolution Based Method for Estimating Local Surface Roughness from Point Clouds. *ISPRS J. Photogramm. Remote Sens.* **2018**, *144*, 369–378. [CrossRef]
90. Woodcock, C.E.; Strahler, A.H. The Factor of Scale in Remote Sensing. *Remote Sens. Environ.* **1987**, *21*, 311–332. [CrossRef]
91. Drăguţ, L.; Eisank, C.; Strasser, T. Local Variance for Multi-Scale Analysis in Geomorphometry. *Geomorphology* **2011**, *130*, 162–172. [CrossRef]
92. Koenderink, J.J. The Structure of Images. *Biol. Cybern.* **1984**, *50*, 363–370. [CrossRef]
93. Lindeberg, T. Scale-Space Theory: A Basic Tool for Analyzing Structures at Different Scales. *J. Appl. Stat.* **1994**, *21*, 225–270. [CrossRef]
94. Fisher, P.; Wood, J.; Cheng, T. Where Is Helvellyn? Fuzziness of Multi-Scale Landscape Morphometry. *Trans. Inst. Br. Geogr.* **2004**, *29*, 106–128. [CrossRef]
95. Trevisani, S.; Cavalli, M.; Marchi, L. Reading the Bed Morphology of a Mountain Stream: A Geomorphometric Study on High-Resolution Topographic Data. *Hydrol. Earth Syst. Sci.* **2010**, *14*, 393–405. [CrossRef]
96. Hani, A.F.M.; Sathyamoorthy, D.; Asirvadam, V.S. A Method for Computation of Surface Roughness of Digital Elevation Model Terrains via Multiscale Analysis. *Comput. Geosci.* **2011**, *37*, 177–192. [CrossRef]
97. Florinsky, I.V. An Illustrated Introduction to General Geomorphometry. *Prog. Phys. Geogr.* **2017**, *41*, 723–752. [CrossRef]
98. Minár, J.; Evans, I.S.; Jenčo, M.A. Comprehensive System of Definitions of Land Surface (Topographic) Curvatures, with Implications for Their Application in Geoscience Modelling and Prediction. *Earth-Sci. Rev.* **2020**, *211*, 103414. [CrossRef]
99. Lindsay, J.B.; Francioni, A.; Cockburn, J.M.H. LiDAR DEM Smoothing and the Preservation of Drainage Features. *Remote Sensing* **2019**, *11*, 1926. [CrossRef]
100. Yu, W.; Zhang, Y.; Ai, T.; Chen, Z. An Integrated Method for DEM Simplification with Terrain Structural Features and Smooth Morphology Preserved. *Int. J. Geogr. Inf. Sci.* **2021**, *35*, 273–295. [CrossRef]
101. Feciskanin, R.; Minár, J. Advancing Raster DEM Generalization with a Quadric Error Metric Approach. *Comput. Geosci.* **2025**, *202*, 105963. [CrossRef]
102. Isaaks, E.H.; Srivastava, R.M. *An Introduction to Applied Geostatistics*; Oxford University Press: Oxford, UK, 1989.
103. Hiller, J.K.; Smith, M. Residual Relief Separation: Digital Elevation Model Enhancement for Geomorphological Mapping. *Earth Surf. Process. Landf.* **2008**, *33*, 2266–2276. [CrossRef]
104. Guisan, A.; Weiss, S.B.; Weiss, A.D. GLM versus CCA Spatial Modeling of Plant Species Distribution. *Plant Ecol.* **1999**, *143*, 107–122. [CrossRef]
105. Wilson, J.P. Digital Terrain Modeling. *Geomorphology* **2012**, *137*, 107–121. [CrossRef]
106. Newman, D.R.; Lindsay, J.B.; Cockburn, J.M.H. Evaluating Metrics of Local Topographic Position for Multiscale Geomorphometric Analysis. *Geomorphology* **2018**, *312*, 40–50. [CrossRef]
107. Majcher, J.; Plets, R.; Quinn, R. Residual Relief Modelling: Digital Elevation Enhancement for Shipwreck Site Characterisation. *Archaeol. Anthropol. Sci.* **2020**, *12*, 122. [CrossRef]

108. Ilich, A.R.; Misiuk, B.; Lecours, V.; Murawski, S.A. MultiscaleDTM: An Open-Source R Package for Multiscale Geomorphometric Analysis. *Trans. GIS* **2023**, *27*, 1164–1204. [CrossRef]
109. Newman, D.R.; Cockburn, J.M.H.; Drăguţ, L.; Lindsay, J.B. Evaluating Scaling Frameworks for Multiscale Geomorphometric Analysis. *Geomatics* **2022**, *2*, 36–51. [CrossRef]
110. Herzfeld, U.C. Vario Functions of Higher Order—Definition and Application to Characterization of Snow Surface Roughness. *Comput. Geosci.* **2002**, *28*, 641–660. [CrossRef]
111. Trevisani, S.; Teza, G.; Guth, P. A Simplified Geostatistical Approach for Characterizing Key Aspects of Short-Range Roughness. *CATENA* **2023**, *223*, 106927. [CrossRef]
112. HOBBS, W.H. Repeating Patterns in the Relief and in the Structure of Land. *GSA Bull.* **1911**, *22*, 123–176. [CrossRef]
113. Drăguţ, L.; Eisank, C. Object Representations at Multiple Scales from Digital Elevation Models. *Geomorphology* **2011**, *129*, 183–189. [CrossRef]
114. Burrough, P.; McDonnell, R. *Principle of Geographic Information Systems*; Oxford University Press: Oxford, UK, 1998.
115. Ojala, T.; Pietikainen, M.; Maenpaa, T. Multiresolution Gray-Scale and Rotation Invariant Texture Classification with Local Binary Patterns. *IEEE Trans. Pattern Anal. Mach. Intell.* **2002**, *24*, 971–987. [CrossRef]
116. Haralick, R.M.; Dinstein, I.; Shanmugam, K. Textural Features for Image Classification. *IEEE Trans. Syst. Man Cybern.* **1973**, *SMC-3*, 610–621. [CrossRef]
117. Jasiewicz, J.; Stepinski, T.F. Geomorphons-a Pattern Recognition Approach to Classification and Mapping of Landforms. *Geomorphology* **2013**, *182*, 147–156. [CrossRef]
118. Adelson, E.H.; Burt, P.J.; Anderson, C.H.; Ogden, J.M.; Bergen, J.R. Pyramid Methods in Image Processing. *RCA Eng.* **1984**, *29*, 33–41.
119. Mallat, S.G. A Theory for Multiresolution Signal Decomposition: The Wavelet Representation. *IEEE Trans. Pattern Anal. Mach. Intell.* **1989**, *11*, 674–693. [CrossRef]
120. Kovesi, P. Fast Almost-Gaussian Filtering. In Proceedings of the 2010 Digital Image Computing: Techniques and Applications, DICTA 2010, Sydney, Australia, 1–3 December 2010; pp. 121–125.
121. Lou, S.; Zeng, W.-H.; Jiang, X.-Q.; Scott, P.J. Robust Filtration Techniques in Geometrical Metrology and Their Comparison. *Int. J. Autom. Comput.* **2013**, *10*, 1–8. [CrossRef]
122. Ding, S.; Chen, X.; Ai, C.; Wang, J.; Yang, H. A Noise-Reduction Algorithm for Raw 3D Point Cloud Data of Asphalt Pavement Surface Texture. *Sci. Rep.* **2024**, *14*, 16633. [CrossRef] [PubMed]
123. Lovejoy, S.; Schertzer, D. Haar Wavelets, Fluctuations and Structure Functions: Convenient Choices for Geophysics. *Nonlinear Process. Geophys.* **2012**, *19*, 513–527. [CrossRef]
124. Lai, L.S.-H.; Booth, A.M.; Duvall, A.R.; Herzig, E. Short Communications: Multiscale Topographic Complexity Analysis with pyTopoComplexity. *EGUsphere* **2024**, *2024*, 1–27. [CrossRef]
125. Trevisani, S.; Rocca, M. MAD: Robust Image Texture Analysis for Applications in High Resolution Geomorphometry. *Comput. Geosci.* **2015**, *81*, 78–92. [CrossRef]
126. Guth, P.; Kane, M. Slope, Aspect, and Hillshade Algorithms for Non-Square Digital Elevation Models. *Trans. GIS* **2021**, *25*, 2309–2332. [CrossRef]
127. Minár, J.; Jenčo, M.; Evans, I.S.; Minár, J., Jr.; Kadlec, M.; Krcho, J.; Pacina, J.; Burian, L.; Benová, A. Third-Order Geomorphometric Variables (Derivatives): Definition, Computation and Utilization of Changes of Curvatures. *Int. J. Geogr. Inf. Sci.* **2013**, *27*, 1381–1402. [CrossRef]
128. Florinsky, I.V. Computation of the Third-order Partial Derivatives from a Digital Elevation Model. *Int. J. Geogr. Inf. Sci.* **2009**, *23*, 213–231. [CrossRef]
129. Bosch, E.H.; Oliver, M.A.; Webster, R. Wavelets and the Generalization of the Variogram. *Math. Geol.* **2004**, *36*, 147–186. [CrossRef]
130. Bosch, E.H.; González, A.P.; Vivas, J.G.; Easley, G.R. Directional Wavelets and a Wavelet Variogram for Two-Dimensional Data. *Math. Geosci.* **2009**, *41*, 611–641. [CrossRef]
131. Trevisani, S.; Teza, G.; Guth, P.L. Hacking the Topographic Ruggedness Index. *Geomorphology* **2023**, *439*, 108838. [CrossRef]
132. Dilts, T.E.; Blum, M.E.; Shoemaker, K.T.; Weisberg, P.J.; Stewart, K.M. Improved Topographic Ruggedness Indices More Accurately Model Fine-Scale Ecological Patterns. *Landsc. Ecol.* **2023**, *38*, 1395–1410. [CrossRef]
133. Hengl, T. Finding the Right Pixel Size. *Comput. Geosci.* **2006**, *32*, 1283–1298. [CrossRef]
134. Hoffman, R.; Krotkov, E. Terrain Roughness Measurement from Elevation Maps. In Proceedings of the 1989 Symposium on Visual Communications, Image Processing, and Intelligent Robotics Systems, Philadelphia, PA, USA, 1–3 November 1989; 1990; 1195, pp. 104–114.
135. Voigtländer, A.; Rheinwalt, A.; Tofelde, S. Quantifying Earth's Topography: Steeper and Larger Than Projected in Digital Terrain Models. *Geophys. Res. Lett.* **2024**, *51*, e2024GL109517. [CrossRef]
136. Milenković, M.; Ressl, C.; Karel, W.; Mandlburger, G.; Pfeifer, N. Roughness Spectra Derived from Multi-Scale LIDAR Point Clouds of a Gravel Surface: A Comparison and Sensitivity Analysis. *ISPRS Int. J. Geo-Inf.* **2018**, *7*, 69. [CrossRef]

137. Jaboyedoff, M.; Bu, F.; Chalé, A.; Choanji, T.; Derron, M.-H.; Fei, L.; Liu, W.; Wolff, C.; Agliardi, F.; Franzosi, F.; et al. Toward the Assessment of the Rockfall Sources Hazard Failure Using 3D Point Clouds and Remote Sensing Techniques. In *New Challenges in Rock Mechanics and Rock Engineering—Proceedings of the ISRM Rock Mechanics Symposium, EUROCK 2024*; CRC Press: Boca Raton, FL, USA, 2024; pp. 39–60.
138. Doane, T.H.; Gearon, J.H.; Martin, H.K.; Yanites, B.J.; Edmonds, D.A. Topographic Roughness as an Emergent Property of Geomorphic Processes and Events. *AGU Adv.* **2024**, *5*, e2024AV001264. [CrossRef]
139. Brodatz, P. *Textures: A Photographic Album for Artists & Designers*; Dover Publications: New York, NY, USA, 1966.
140. Routray, P.K.; Kanade, A.S.; Tiwari, K.; Pounds, P.; Muniyandi, M. Towards Multidimensional Textural Perception and Classification Through Whisker. In Proceedings of the 2022 IEEE International Symposium on Robotic and Sensors Environments (ROSE), Abu Dhabi, United Arab Emirates, 14–15 November 2022; pp. 1–7.
141. Volume 1: Textures (USC Viterbi School of Engineering). Available online: https://sipi.usc.edu/database/database.php?volume=textures (accessed on 25 November 2025).
142. Sarkar, N.; Chaudhuri, B.B. An Efficient Approach to Estimate Fractal Dimension of Textural Images. *Pattern Recognit.* **1992**, *25*, 1035–1041. [CrossRef]
143. Randen, T.; Husoy, J. Filtering for Texture Classification: A Comparative Study. *IEEE Trans. Pattern Anal. Mach. Intell.* **1999**, *21*, 291–310. [CrossRef]
144. Maillard, P. Comparing Texture Analysis Methods through Classification. *Comp. Texture Anal. Methods Through Classif.* **2003**, *4*, 357–367. [CrossRef]
145. Copernicus DEM 30 m. Available online: https://doi.org/10.5270/esa-c5d3d65 (accessed on 25 November 2025).
146. Bielski, C.; Lopez-Vazquez, C.; Grohmann, C.H.; Guth, P.L.; Hawker, L.; Gesch, D.; Trevisani, S.; Herrera-Cruz, V.; Riazanoff, S.; Corseaux, A.; et al. Novel Approach for Ranking DEMs: Copernicus DEM Improves One Arc Second Open Global Topography. *IEEE Trans. Geosci. Remote Sens.* **2024**, *62*, 4503922. [CrossRef]
147. Guth, P.L.; Trevisani, S.; Grohmann, C.H.; Lindsay, J.; Gesch, D.; Hawker, L.; Bielski, C. Ranking of 10 Global One-Arc-Second DEMs Reveals Limitations in Terrain Morphology Representation. *Remote Sens.* **2024**, *16*, 3273. [CrossRef]
148. Jasiewicz, J.; Netzel, P.; Stepinski, T.F. Landscape Similarity, Retrieval, and Machine Mapping of Physiographic Units. *Geomorphology* **2014**, *221*, 104–112. [CrossRef]
149. Jasiewicz, J.; Netzel, P.; Stepinski, T. GeoPAT: A Toolbox for Pattern-Based Information Retrieval from Large Geospatial Databases. *Comput. Geosci.* **2015**, *80*, 62–73. [CrossRef]
150. Bertin, S.; Friedrich, H.; Delmas, P.; Chan, E.; Gimel'farb, G. DEM Quality Assessment with a 3D Printed Gravel Bed Applied to Stereo Photogrammetry. *Photogramm. Rec.* **2014**, *29*, 241–264. [CrossRef]
151. Hillier, J.K.; Sofia, G.; Conway, S.J. Perspective—Synthetic DEMs: A Vital Underpinning for the Quantitative Future of Landform Analysis? *Earth Surf. Dyn.* **2015**, *3*, 587–598. [CrossRef]
152. Guérin, É.; Digne, J.; Galin, É.; Peytavie, A.; Wolf, C.; Benes, B.; Martinez, B. Interactive Example-Based Terrain Authoring with Conditional Generative Adversarial Networks. *ACM Trans. Graph.* **2017**, *36*, 228. [CrossRef]
153. Wang, F.; Liu, H.; Samaras, D.; Chen, C. TopoGAN: A Topology-Aware Generative Adversarial Network. In Proceedings of the Computer Vision—ECCV 2020, Glasgow, UK, 23–28 August 2020; Vedaldi, A., Bischof, H., Brox, T., Frahm, J.-M., Eds.; Springer International Publishing: Cham, Switzerland, 2020; pp. 118–136.
154. Temme, A.J.A.M.; Schoorl, J.M.; Claessens, L.; Veldkamp, A. 10.11—Quantitative Modeling of Landscape Evolution. In *Treatise on Geomorphology*, 2nd ed.; Shroder, J.F., Ed.; Academic Press: Oxford, UK, 2022; pp. 162–183. ISBN 978-0-12-818235-2.
155. Conrad, O.; Bechtel, B.; Bock, M.; Dietrich, H.; Fischer, E.; Gerlitz, L.; Wehberg, J.; Wichmann, V.; Böhner, J. System for Automated Geoscientific Analyses (SAGA) v. 2.1.4. *Geosci. Model Dev.* **2015**, *8*, 1991–2007. [CrossRef]
156. Wilson, J.P.; Gallant, J.C. *Terrain Analysis: Principles and Applications*; John Wiley & Sons: Hoboken, NJ, USA, 2000.
157. Jenness, J.S. Calculating Landscape Surface Area from Digital Elevation Models. *Wildl. Soc. Bull.* **2004**, *32*, 829–839. [CrossRef]
158. Woodcock, N.H. Specification of Fabric Shapes Using an Eigenvalue Method. *Bull. Geol. Soc. Am.* **1977**, *88*, 1231–1236. [CrossRef]
159. Dóniz-Páez, J.; Beltrán-Yanes, E.; Becerra-Ramírez, R.; Pérez, N.M.; Hernández, P.A.; Hernández, W. Diversity of Volcanic Geoheritage in the Canary Islands, Spain. *Geosciences* **2020**, *10*, 390. [CrossRef]
160. Spain Lidar III Coverage. Available online: https://centrodedescargas.cnig.es/CentroDescargas/lidar-tercera-cobertura (accessed on 25 November 2025).
161. Trevisani, S. *Lazarote DTM and RGB Imagery [Dataset]*; Zenodo: Geneva, Switzerland, 2025. [CrossRef]
162. Garnier, S.; Ross, N.; Rudis, R.; Camargo, P.A.; Sciaini, M. *Viridis(Lite)—Colorblind-Friendly Color Maps for R*; R Foundation for Statistical Computing: Vienna, Austria, 2024.
163. Favalli, M.; Fornaciai, A. Visualization and Comparison of DEM-Derived Parameters. Application to Volcanic Areas. *Geomorphology* **2017**, *290*, 69–84. [CrossRef]
164. Atkinson, P.M.; Lewis, P. Geostatistical Classification for Remote Sensing: An Introduction. *Comput. Geosci.* **2000**, *26*, 361–371. [CrossRef]

165. Bretar, F.; Arab-Sedze, M.; Champion, J.; Pierrot-Deseilligny, M.; Heggy, E.; Jacquemoud, S. An Advanced Photogrammetric Method to Measure Surface Roughness: Application to Volcanic Terrains in the Piton de La Fournaise, Reunion Island. *Remote Sens. Environ.* **2013**, *135*, 1–11. [CrossRef]
166. Roy, S.G.; Koons, P.O.; Osti, B.; Upton, P.; Tucker, G.E. Multi-Scale Characterization of Topographic Anisotropy. *Comput. Geosci.* **2016**, *90*, 102–116. [CrossRef]
167. Newman, D.R.; Lindsay, J.B.; Cockburn, J.M.H. Measuring Hyperscale Topographic Anisotropy as a Continuous Landscape Property. *Geosciences* **2018**, *8*, 278. [CrossRef]
168. Dichiarante, A.M.; Torgersen, E.; Redfield, T.; Köhler, A.; Torabi, A.; Svendby, K.; Oye, V. Spectral Analysis of Topography as Proxy for Lineament Analysis. *J. Geophys. Res. Solid Earth* **2025**, *130*, e2024JB029790. [CrossRef]
169. Trevisani, S.; Cavalli, M. Topography-Based Flow-Directional Roughness: Potential and Challenges. *Earth Surf. Dyn.* **2016**, *4*, 343–358. [CrossRef]
170. Hall-Beyer, M. Practical Guidelines for Choosing GLCM Textures to Use in Landscape Classification Tasks over a Range of Moderate Spatial Scales. *Int. J. Remote Sens.* **2017**, *38*, 1312–1338. [CrossRef]
171. Ilich, A.R. *GLCMTextures*; Zenodo: Geneva, Switzerland, 2020. [CrossRef]
172. Melton, M.A. Correlation Structure of Morphometric Properties of Drainage Systems and Their Controlling Agents. *J. Geol.* **1958**, *66*, 442–460. [CrossRef]
173. Reis, I.L.; Marinho, G.S.; da Silva Rios, G.; Santana, D.B.; Lense, G.H.E.; Mincato, R.L.; Rubira, F.G. Morphometric Parameters of the Relief and Drainage Network of the Formiga River Subbasin, Minas Gerais, Brazil; [Parâmetros Morfométricos Do Relevo e Da Rede de Drenagem Da Sub-Bacia Hidrográfica Do Rio Formiga, Minas Gerais, Brasil]. *Rev. Bras. Geomorfol.* **2023**, *24*. [CrossRef]
174. McGarigal, K.; Cushman, S.A. The Gradient Concept of Landscape Structure. In *Issues and Perspectives in Landscape Ecology*; Cambridge University Press: Cambridge, UK, 2005.
175. Hesselbarth, M.H.K.; Sciaini, M.; With, K.A.; Wiegand, K.; Nowosad, J. Landscapemetrics: An Open-Source R Tool to Calculate Landscape Metrics. *Ecography* **2019**, *42*, 1648–1657. [CrossRef]
176. Nadachowski, P.; Lubniewski, Z.; Lysakowska, A.M.; Trzcinska, K.; Wroblewski, R.; Tegowski, J. Classification of Glacial and Fluvioglacial Landforms by Convolutional Neural Networks Using a Digital Elevation Model. *IEEE J. Sel. Top. Appl. Earth Obs. Remote Sens.* **2024**, *17*, 18549–18565. [CrossRef]
177. Kudaibergenov, M.; Nurakynov, S.; Iskakov, B.; Iskaliyeva, G.; Maksum, Y.; Orynbassarova, E.; Akhmetov, B.; Sydyk, N. Application of Artificial Intelligence in Landslide Susceptibility Assessment: Review of Recent Progress. *Remote Sens.* **2025**, *17*, 34. [CrossRef]
178. Şeflek, A.Y.; Büyükarıkan, B.; Dokumacı, K.Y. Evaluation of a Newly Developed Ploughshare: An Ensemble Deep Learning Approach for Soil Surface Roughness Classification with Explainable Artificial Intelligence. *Eng. Appl. Artif. Intell.* **2025**, *159*, 111739. [CrossRef]
179. Argudo, O.; Guérin, E.; Schott, H.; Galin, E. Terrain Descriptors for Landscape Synthesis, Analysis and Simulation. *Comput. Graph. Forum* **2025**, *44*, e70080. [CrossRef]
180. Malik, K.; Robertson, C. Landscape Similarity Analysis Using Texture Encoded Deep-Learning Features on Unclassified Remote Sensing Imagery. *Remote Sens.* **2021**, *13*, 492. [CrossRef]
181. Strobl, P. The New Copernicus Digital Elevation Model. *GSICS Q.* **2020**, *14*, 17–18.
182. Trevisani, S. Atlas Surface Texture Prototyping. 2025. Available online: https://Github.Com/Strevisani/Atlas-of-Surface-Textures (accessed on 25 November 2025).
183. Kennelly, P.J.; Patterson, T.; Jenny, B.; Huffman, D.P.; Marston, B.E.; Bell, S.; Tait, A.M. Elevation Models for Reproducible Evaluation of Terrain Representation. *Cartogr. Geogr. Inf. Sci.* **2021**, *48*, 63–77. [CrossRef]
184. Kennelly, P.J.; Patterson, T.; Jenny, B.; Huffman, D.P.; Marston, B.E.; Bell, S.; Tait, A.M. *Elevation Models for Reproducible Evaluation of Terrain Representation—Archetypal Landforms [Data Set Version 2.0]*; Zenodo: Geneva, Switzerland, 2020.